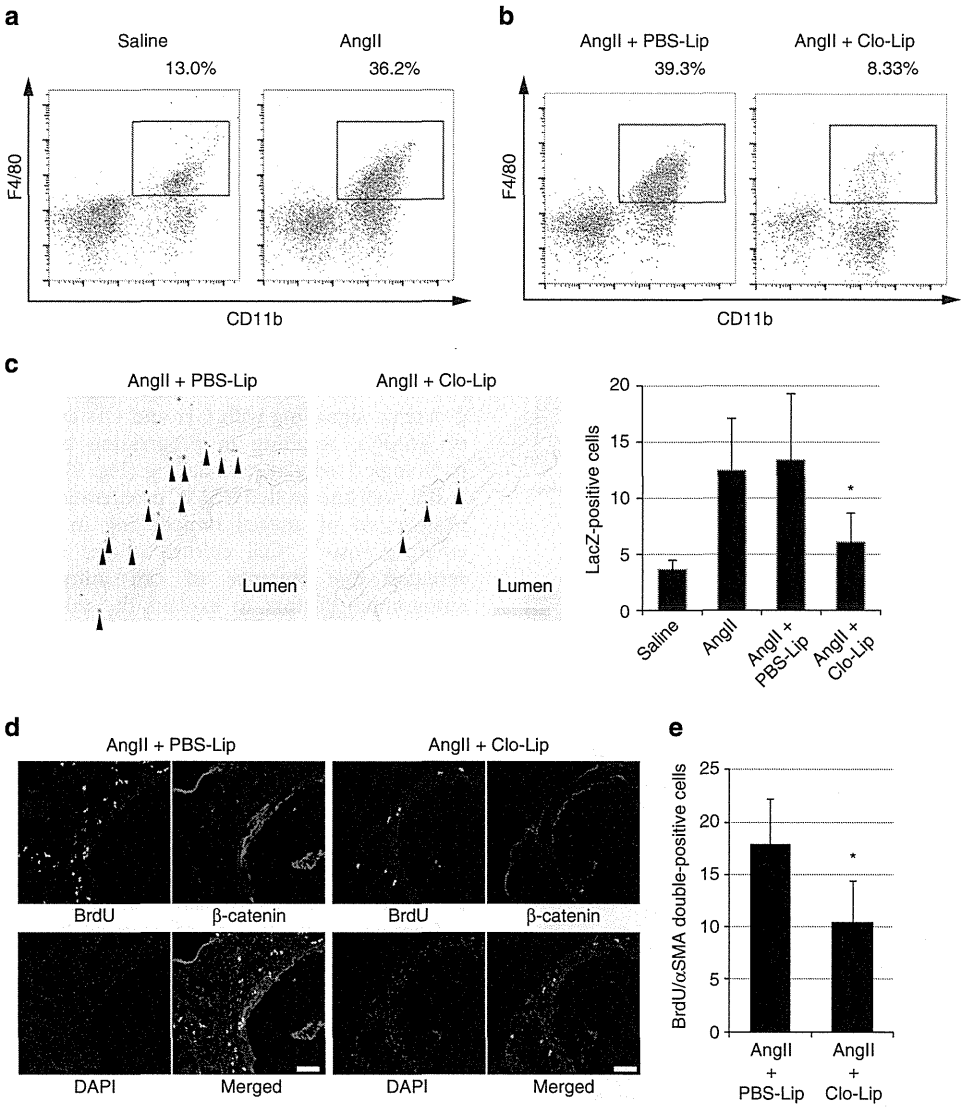

Figure 5 | Recruited Mϕs activate β-catenin signalling and induce VSMC proliferation after AngII infusion. (**a**,**b**) Representative density plots. Aortic Mϕs of 1-week saline- and AngII-infused mice (**a**) of and in AngII-infused mice treated with PBS liposome (PBS-Lip) or clodronate liposome (Clo-Lip) (**b**) were analysed by flow cytometry. Cells within the boxes are CD11b + F4/80 + Mϕs. The flow cytometric analysis was performed with pooled aortic tissues from a total of 3–10 mice and percent gated cell frequencies are indicated in each representative plot. (**c**) β-Galactosidase staining of the aortic tissue from AngII-infused $Axin2^{LacZ}$ mice, treated with PBS-Lip or Clo-Lip. Arrowheads indicate β-galactosidase-positive nuclei. Scale bar, 50 μm. The number of LacZ-positive cells in the media of aortic tissue from $Axin2^{LacZ}$ mice is shown. *$P<0.05$ versus PBS-Lip-treated AngII-infused mice ($n=5$–6). (**d**) Aortic tissues from AngII-infused mice treated with PBS-Lip or Clo-Lip were immunostained for BrdU (green) and β-catenin (red). Scale bar, 100 μm. (**e**) The number of double-positive (BrdU(+)/αSMA(+)) cells per aortic section from AngII-infused mice treated with PBS-Lip or Clo-Lip. *$P<0.05$ versus PBS-Lip-treated AngII-infused mice ($n=5$). Statistical significance was determined using one-way analysis of variance with Turkey's *post hoc* test for **c**, and the unpaired two-tailed Mann–Whitney *U*-test for **e**. Results are represented as mean ± s.d. DAPI, 4′,6-diamidino-2-phenylindole.

complex, which is composed of C1q, C1r and C1s, also activated β-catenin signalling in HASMCs, and this effect was inhibited by C1-INH (Supplementary Fig. 5b). WB analysis of cell culture media revealed that both C1r and C1s were secreted from HASMCs but not from Mϕs (Supplementary Fig. 5c,d). Activation of β-catenin signalling and proliferation of HASMCs induced by M2 Mϕ-CM was prevented by C1-INH (Fig. 7e,f; Supplementary Fig. 5e,f). These results collectively suggest that the C1 complex, which is composed of M2 Mϕ-derived C1q and VSMC-derived C1r/s is the factor that activates β-catenin signalling and induces proliferation of VSMCs.

C1-induced β-catenin signalling causes arterial remodelling. We next examined whether C1 is responsible for hypertension-induced activation of β-catenin signalling and proliferation of VSMCs *in vivo*. Expression levels of *C1qa*, *C1ra* and *C1s* genes were increased in the aortic tissue 1 week after AngII infusion (Fig. 8a). Aortic Mϕs increased *C1qa* gene expression, but not *C1ra* and *C1s*, 1 week after AngII infusion (Fig. 8b). Treatment with C1-INH prevented the activation of β-catenin signalling in aortic VSMCs and suppressed proliferation of VSMCs induced by AngII infusion (Fig. 8c,d; Supplementary Fig. 6a). In addition, activation of β-catenin signalling and proliferation of VSMCs were both attenuated in C1qa-deficient

mice but not in C3-deficient mice at 1 week after AngII infusion (Fig. 8e,f; Supplementary Fig. 6b,c), indicating that these phenotypes induced by C1 are independent of complement cascade activation. There was no significant difference in blood pressure among all groups of mice (Supplementary Fig. 3f). The size of the VSMCs following AngII infusion was comparable between wild-type and C1qa-deficient mice (Supplementary Fig. 6d). Arterial remodelling at 6 weeks after AngII infusion was attenuated in C1qa-deficient mice compared with wild-type mice (Fig. 8g; Supplementary Fig. 6e,f), suggesting that C1-induced activation of β-catenin signalling, but not C1-induced activation of the classical complement cascade, mediates VSMC proliferation and hypertensive arterial remodelling.

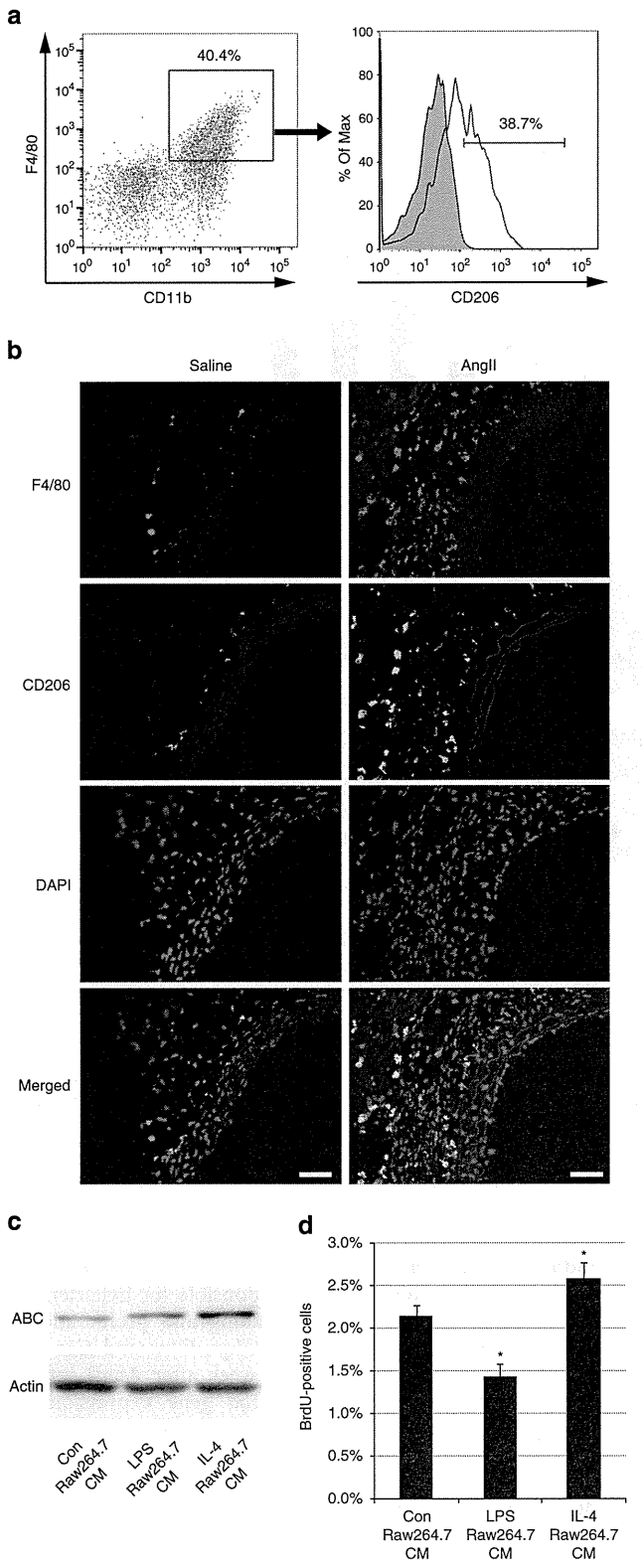

Discussion

In this study, we have elucidated the novel molecular and cellular interplay that initiates hypertensive arterial remodelling. Mϕs were recruited into the aortic adventitia soon after blood-pressure elevation and secreted complement C1q, which activated β-catenin signalling with C1r and C1s and induced proliferation of VSMCs, resulting in progression of hypertension-induced pathological arterial remodelling (Fig. 9).

It is well known that VSMC proliferation plays a key role in the progression of arterial remodelling in hypertension[31] and in atherosclerosis[32]. Cell culture studies using hypertensive rats revealed the presence of cell autonomous and non-cell autonomous factors to explain the mitotic nature of VSMCs during hypertension[7,33]. Various growth factors and G-protein-coupled receptor agonists have been shown to induce proliferation of VSMCs in a non-cell autonomous manner. Most of these mitogenic stimuli activate mitogen-activated protein kinases, especially ERKs[6,20]. In the present study, AngII-induced activation of ERKs was not sufficient to promote VSMC proliferation *in vitro*. We also found no activation of ERKs in the aortic tissue 1 week after AngII infusion when the VSMC proliferation was already observed, suggesting that ERKs are not involved in VSMC proliferation at the initial stage of hypertensive arterial remodelling (Supplementary Fig. 1a–c).

Compared with the critical roles of Wnt/β-catenin signalling during embryonic angiogenesis[34], its role during the postnatal period is less investigated. Activation of β-catenin signalling in intimal thickening has been reported[14,15]; however, these results have been derived from a specific situation such as after the acute ligation of the arteries or the direct mechanical injury to the arterial lumen. In the present study, we showed the activation of β-catenin signalling in a mice model of AngII-induced blood-pressure elevation, which is more physiological than previous reports. Inhibition of β-catenin signalling ameliorated the effect of high blood pressure on VSMC proliferation, suggesting the critical role of β-catenin signalling as a regulator of arterial remodelling during the postnatal period.

Vascular inflammation is a well-known pathogenic feature in arterial remodelling during hypertension and atherosclerosis[4–6].

Figure 6 | M2-type Mϕs are the key players that activate β-catenin signalling during hypertension. (**a**) Representative density plots and histogram. Aortic CD11b+F4/80+ Mϕs in AngII-infused mice were further analysed for CD206 positivity. The shaded histogram indicates an isotype-control stained sample. (**b**) Aortic tissues from saline- or AngII-infused mice were immunostained for CD206 (green) and F4/80 (red). Scale bar, 50 μm. (**c**) Representative western blot analysis. Conditioned media from Raw264.7 cells treated with PBS (Con Raw264.7 CM), LPS (50 ng ml^{-1}) (LPS Raw264.7 CM) or IL-4 (20 ng ml^{-1}) (IL-4 Raw264.7 CM) were added to HASMCs, and the amount of ABC in the total cell lysate of HASMCs was analysed. (**d**) HASMCs were treated as in **c**, and the percentage of BrdU-positive cells was counted. *$P<0.05$ versus Con Raw264.7 CM ($n=4$). Statistical significance was determined using one-way analysis of variance with Turkey's *post hoc* test for **d**. Results are represented as mean ± s.d. DAPI, 4′,6-diamidino-2-phenylindole.

A massive recruitment of Mϕs to the adventitia of the aortic wall after AngII infusion was consistent with previous reports[35,36]. It remains unclear which type of Mϕs is involved in hypertensive arterial remodelling. We elucidated that the anti-inflammatory (M2) phenotype but not pro-inflammatory (M1) phenotype was the prevailing characteristic of aortic Mϕs that infiltrates into aortic adventitia soon after blood-pressure elevation (Fig. 6a,b). M2-polarized Mϕs secreted a factor that induces proliferation of VSMCs by activating β-catenin signalling, and one of the potent candidates was C1q. We have reported that complement C1q activates β-catenin signalling through C1s-dependent enzymatic cleavage of LRP6 (ref. 16). Here, we revealed that M2-type

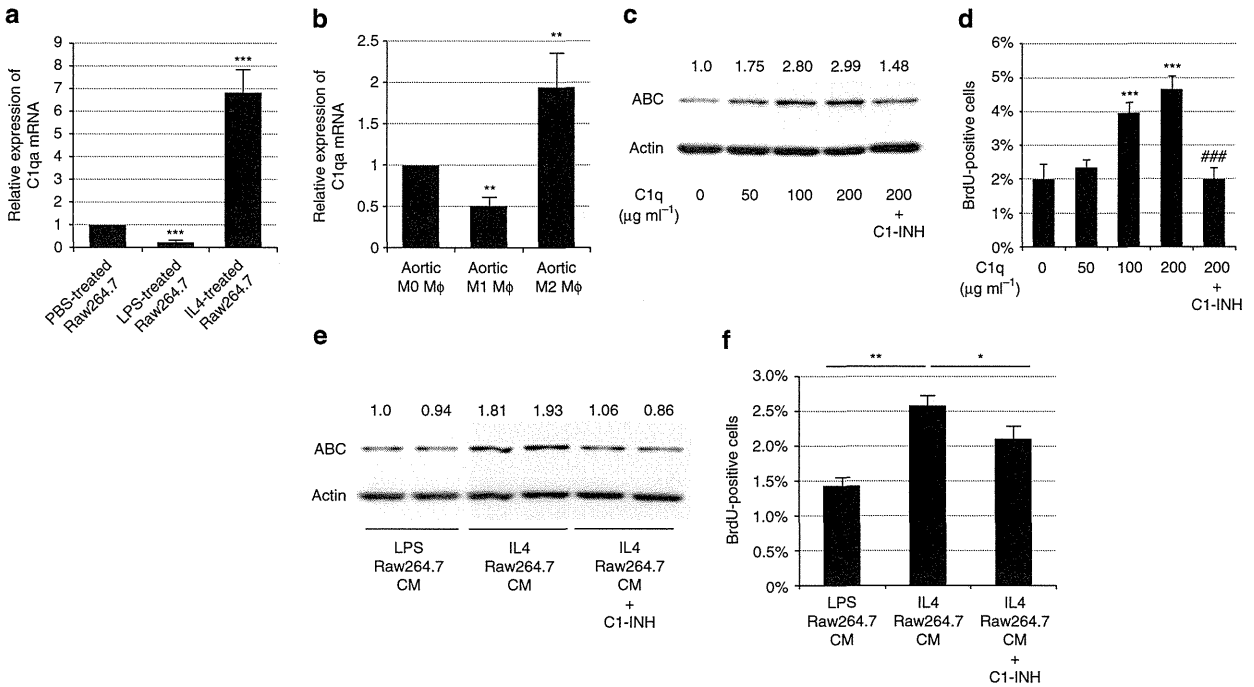

Figure 7 | C1q secreted from M2-type Mϕs activates β-catenin signalling and induces VSMC proliferation. (**a**) Real-time PCR analysis for the expression level of *C1qa* gene in Raw264.7 cells treated with PBS, LPS (50 ng ml^{-1}) or IL-4 (20 ng ml^{-1}). The values are shown as fold induction over PBS-treated Raw264.7 cells. ***$P<0.001$ versus PBS-treated Raw264.7 cells ($n=4$). (**b**) M0, M1 and M2 Mϕs from 10 pooled aortic tissues from AngII-infused mice were sorted by flow cytometry and the expression level of *C1qa* gene was analysed by real-time PCR. The values are shown as fold induction over aortic M0 Mϕs ($n=4$). (**c**) Representative western blot analysis. HASMCs were treated with C1q (50, 100 and 200 μg ml^{-1}) and C1-INH (150 μg ml^{-1}). The protein amount of ABC was analysed and the relative intensity of each band is shown over each immunoblot after normalization for the level of actin. (**d**) HASMCs were treated as in **c**, and the number of BrdU-positive cells was counted. ***$P<0.001$ versus non-treated cells (C1q 0 μg ml^{-1}) ($n=4$), ###$P<0.001$ versus C1q (200 μg ml^{-1}) treated cells. (**e**) Representative western blot analysis. Conditioned media from Raw264.7 cells treated with LPS (50 ng ml^{-1}) (LPS Raw264.7 CM) or IL-4 (20 ng ml^{-1}) (IL-4 Raw264.7 CM) were added to HASMCs with or without C1-INH (150 μg ml^{-1}). The protein amount of ABC in the total cell lysate of HASMCs was analysed and the relative intensity of each band is shown over each immunoblot after normalization for the level of actin. (**f**) HASMCs were treated as in **e**, and the number of BrdU-positive cells was counted ($n=4$). **$P<0.01$ versus LPS Raw264.7 CM. *$P<0.05$ versus IL-4 Raw264.7 CM. Statistical significance was determined using one-way analysis of variance with Turkey's *post hoc* test. Results are represented as mean ± s.d. mRNA, messenger RNA.

Figure 8 | C1q mediates AngII-induced activation of β-catenin signalling and arterial remodelling. (**a**) Real-time PCR analysis for the expression levels of *C1qa, C1ra and C1s* genes in the aortic tissue from 1-week saline- or AngII-infused mice. Values are shown as fold induction over saline-infused mice. **$P<0.01$ versus saline-infused mice ($n=6$). (**b**) Real-time PCR analysis for the expression levels of *C1qa, C1ra and C1s* genes in aortic Mϕs sorted by flow cytometry from 1-week saline- or AngII-infused mice. The values are shown as fold induction over aortic Mϕs isolated from saline-infused mice (saline AoMp). *$P<0.05$, **$P<0.01$ versus saline AoMp ($n=4$). (**c**) Aortic tissues from 1-week AngII-infused mice treated with PBS or with C1-INH were immunostained for BrdU (green) and β-catenin (red). Scale bar, 100 μm. (**d**) The number of double-positive (BrdU(+)/αSMA(+)) cells per section. *$P<0.05$ versus AngII-infused mice treated with PBS ($n=8$). (**e**) Aortic tissues from AngII-infused wild-type mice (WT AngII), C1qa-deficient mice (C1qKO AngII) and C3-deficient (C3KO AngII) mice were immunostained for BrdU (green) and β-catenin (red). Scale bar, 100 μm. (**f**) The number of double-positive (BrdU(+)/αSMA(+)) cells per section. **$P<0.01$ versus 1-week AngII-infused wild-type mice ($n=4$–7). NS, not significant. (**g**) Morphometric analysis. Aortic tissues from WT mice or C1qKO mice after saline- or AngII-infusion were immunostained for αSMA and the vessel diameter was measured using ImageJ. *$P<0.05$ versus 6-week AngII-infused WT mice ($n=5$–9). Statistical significance was determined using the unpaired two-tailed Mann–Whitney *U*-test for **a** and **b**, the Kruskal–Wallis test with Dunn's correction for multiple comparison for **d**, one-way analysis of variance (ANOVA) with Turkey's *post hoc* test for **f** and the two-way ANOVA followed by Tukey's multiple comparisons test for **g**. Results are represented as mean ± s.d. DAPI, 4′,6-diamidino-2-phenylindole.

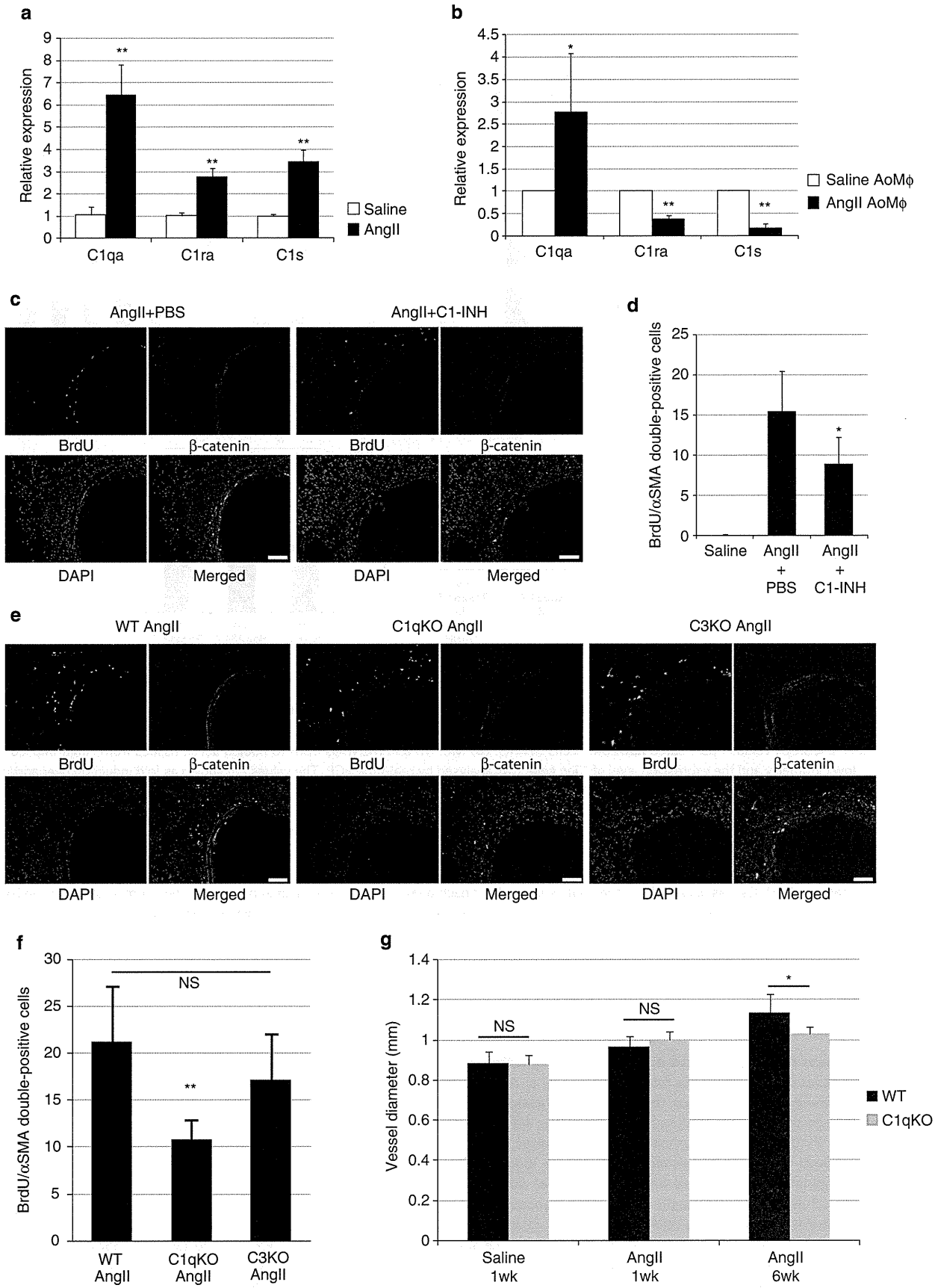

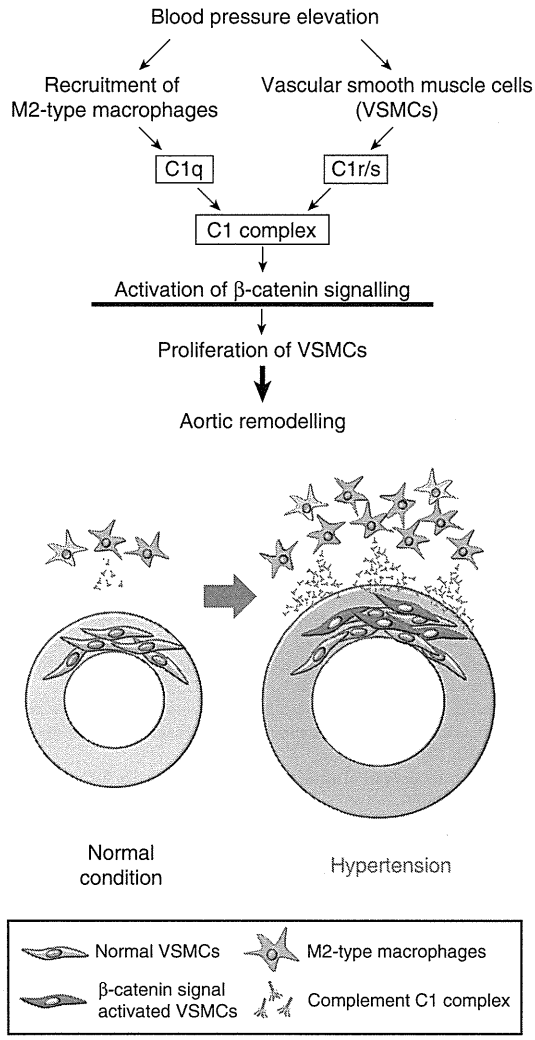

Figure 9 | Mechanisms of hypertensive arterial remodelling. M2-type Mϕs are recruited to the aortic adventitia after blood-pressure elevation and secrete C1q. Mϕ-derived C1q and VSMC-derived C1r/s might compose the C1 complex, which plays a pivotal role in initiating hypertensive arterial remodelling through activating β-catenin signalling in VSMCs and inducing proliferation of VSMCs.

Mϕ-derived C1q and VSMC-derived C1r/s might compose the C1 complex and activate β-catenin signalling in VSMCs (Fig. 9).

In the previous report, we showed that C1q is the molecule that is increased in the blood by aging and activates β-catenin signalling. Here we first demonstrated that the C1 complex activates β-catenin signalling and induces proliferation of VSMCs during the early stage of hypertension, which leads to arterial remodelling at the later stage.

It was previously reported that C1-INH treatment blocked neointima formation following arterial injury in atherosclerotic mice[37], indicating that C1q progresses injury-induced arterial remodelling. Conversely, Mϕ infiltration into plaque and progression of atherosclerotic plaque formation in low-density lipoprotein receptor-deficient mice were exaggerated by additional *C1qa* gene disruption[38]. This evidence suggests that C1q might also mediate anti-inflammatory and anti-atherosclerotic effects in arterial plaque progression. Together with our findings, the role of C1 or C1q in arterial remodelling may differ depending on its aetiology. In addition, the genetic or pharmacologic loss-of-function experiments did not completely inhibit proliferation of VSMCs after AngII infusion, suggesting that pathways other than the C1-β-catenin pathway are also involved in this phenomenon.

Our findings provide a novel mechanistic link between humoral innate immunity and arterial remodelling, and suggest that blocking C1-induced activation of β-catenin signalling becomes a novel therapeutic strategy to prevent arteriosclerosis associated with hypertension.

Methods

Reagents. BrdU, tamoxifen and clodronate disodium were purchased from Sigma. Human complement C1q and C1 complexes were from Calbiochem. AngII and hydralazine hydrochloride were from Wako. C1-INH (Berinert) was from CSL Behring. PKF115-584 (ref. 22) was from Novartis. Human recombinant Wnt3A was from R&D. Mouse recombinant IL-4 was from PeproTech. Mouse monoclonal antibody (14/Beta-Catenin) against β-catenin was from BD Transduction Laboratories (immunofluorescence (IF) dilution 1:200). Rat monoclonal antibody (clone CI:A3-1) against mouse F4/80 (IF dilution 1:50), rabbit monoclonal antibody (clone E247) against β-catenin (WB dilution 1:2,000), rabbit polyclonal antibody against axin2 (WB dilution 1:2,000, IF dilution 1:100) and rat monoclonal antibody against BrdU (clone BU1 75(ICR1)) (IF dilution 1:200) were from Abcam. Mouse monoclonal antibody (clone 8E7) against ABC was from Millipore (WB dilution 1:1,000). Rabbit polyclonal antibody against actin and alpha-smooth muscle actin (αSMA) were from Sigma (IF dilution 1:200). TACS 2TdT Fluorescein Kit was from Trevigen. Mouse monoclonal antibodies against C1r (WB dilution 1:250) and C1s (WB dilution 1:250) were from R&D. Secondary antibodies conjugated to Alexa Fluor 488 and Alexa Fluor 546 were from Molecular Probes (IF dilution 1:200).

Animals. Male mice 8–10 weeks of age were used for all experiments. C57BL/6 mice were purchased from CLEA Japan. $Axin2^{LacZ}$ mice[11] were from the Jackson laboratory. C1qa knockout mice[39], C3 knockout mice[40] and SMMHC-$CreER^{T2}$ mice[23] were previously described, and mice backcrossed into C57BL/6 background were used for experiments. Conditional β-catenin knockout mice (*Ctnnb1*$^{flox/flox}$ mice) were established as previously described[41]. For AngII infusion, an osmotic minipump (Alzet) containing either saline or AngII (1.8 μg kg^{-1} min^{-1}) was implanted subcutaneously. Blood pressure was measured in conscious mice by the tail-cuff system using BP98A (Softron) according to the manufacturer's protocol. To induce Cre/loxP-mediated gene disruption in SMMHC-$CreER^{T2}$ mice, tamoxifen dissolved in corn oil was injected intraperitoneally for 5 consecutive days (1 mg per day). Hydralazine was administered in drinking water (250 mg l^{-1}) 1 week before the implantation of an osmotic minipump, and the solution was replaced every single day. Control mice received drinking water alone. Clodronate disodium was encapsulated into liposomes by Katayama Chemical Industries Co., Ltd (Osaka, Japan). Clodronate liposomes were prepared by freeze–thawing and filter extrusion. Dipalmitoylphosphatidylcholine, cholesterol and dipalmitoylphosphatidylserine were mixed at the molar ratio 50:40:10. The dry lipid mixture was solubilized in PBS or clodronate. The resulting vesicles were freeze–thawed in liquid nitrogen and water at 40°C, followed by filter extrusion through 400-nm membranes (Nuclepore, Sterico, Dietikon, Switzerland) using the Lipex extruder (Lipex Biomembranes Inc., Vancouver, Canada). The suspension was ultrafiltrated using PBS through an Amicon XM300 membrane to remove free clodronate. The size of liposome was measured by dynamic light-scattering spectrophotometry (Zetasizer Nano-ZS, Malvern, Worcestershire, UK) at 25°C. Clodronate liposomes contain ~10 mg clodronate per ml and have a mean diameter of 250 ± 50 nm. PBS liposomes or clodronate liposomes (200 μl) were administered intravenously 3 days before the implantation of an osmotic minipump and every 3 days thereafter. Dimethylsulphoxide (DMSO) or PKF115-584 (0.16 mg kg^{-1}) was administered every other day via intraperitoneal injections from 5 days before the implantation of an osmotic minipump. PBS or C1-INH (15 U per day) was administered intravenously 5 days before the implantation of an osmotic minipump and every other day thereafter. All experiments were approved by the University of Tokyo Ethics Committee for Animal Experiments and strictly adhered to the guidelines for animal experiments of the University of Tokyo.

Cell culture. HASMCs were cultured in smooth muscle growth medium-2 (Lonza), which contains fetal bovine serum (FBS) and various growth factors, and starved for 24 h before stimulation in smooth muscle basal medium-2 (Lonza) devoid of serum or growth factors. Raw264.7 cells were purchased from American Type Culture Collection and cultured in Dulbecco's modified Eagle's medium supplemented with 10% FBS. BMDMs were isolated from femurs of wild-type mice and cultured in Mϕ medium (RPMI 1640 medium supplemented with 10% FBS, 40 ng ml^{-1} murine Macrophage Colony-Stimulating Factor (M-CSF), 2 mM L-glutamine, 50 U ml^{-1} penicillin and 100 μg ml^{-1} streptomycin). For M1 or M2 polarization, Raw264.7 cells or BMDMs were treated with LPS (50 ng ml^{-1}) or IL-4 (20 ng ml^{-1}) for 24 h, respectively. CM of Raw264.7 cells or BMDMs were collected after another 24 h.

RNA analysis. Total RNA was extracted using TRIzol reagent (Invitrogen) according to the manufacturer's instructions. RNA was treated with DNase and reverse transcribed using the QuantiTect Reverse Transcription Kit (Qiagen). Real-time quantitative PCR was performed using the Universal Probe Library (UPL) (Roche) and Light Cycler TaqMan Master kit (Roche). Relative levels of gene expression were normalized to the *Gapdh* gene expression using the comparative Ct method. Primer sequences and the corresponding UPL numbers were designed using an online program provided by Roche. Primer sequences are provided in Supplementary Table 1.

Protein analysis. Abdominal aorta (between the diaphragm and the left renal artery) was minced and lysed in buffer containing 20 mM HEPES (pH: 7.9), 150 mM NaCl, 5 mM EDTA, 15% glycerol, 1% Triton X-100, a protease inhibitor cocktail and phosphatase inhibitor cocktail. Total cell lysate of the cultured cells was lysed in the same buffer. Cytosolic fraction of the cultured cells was obtained using ultracentrifuge. Culture media was concentrated using Amicon Ultra 30 K (Millipore). The proteins were fractioned using 8–10% SDS–polyacrylamide gel electrophoresis and analysed using immunoblotting. Densitometry analysis on the bands was calculated using ImageJ. The non-cropped blots for the representative images are displayed in Supplementary Fig. 7.

Cell proliferation. In cell culture experiments, cells were labelled by adding BrdU (10 μM) to the culture media for 12 h. Cells were then immunostained with anti-BrdU antibody. The percentage of BrdU-positive cells in nine randomly chosen low power fields were calculated for each sample. In mice experiments, BrdU (100 mg kg^{-1}) was injected intraperitoneally 24 h before euthanization. Dissected aortic tissues were embedded in Tissue-Tek® O.C.T.™ (Optimal Cutting Temperature) Compound (SAKURA) and sectioned at 5 μm thickness. After immunostaining with anti-BrdU (1:200) and anti-αSMA (1:200) antibodies, the number of double-positive (BrdU(+)/αSMA(+)) cells per each section was counted. Six sections were examined for each animal and the mean number was shown.

Histological analysis. For morphological analysis, aortic tissues were fixed with formaldehyde and embedded in paraffin. For fluorescent immunostaining, 5-μm-thick fresh-frozen sections were stained and the nuclei were counterstained with 4′,6-diamidino-2-phenylindole. Images were acquired using the LSM510 or LSM700 confocal microscope (Zeiss) or FSX100 (Olympus) and analysed using ImageJ.

Flow cytometric analysis of the aortic tissue. Aortic tissues were minced and digested in digestion solution containing Elastase (Worthington) (0.25 mg ml^{-1}) and LiberaseTH (Roche) (0.025 mg ml^{-1}). Digested tissues were further dissociated with a 21-G needle. Remaining deposited debris was removed and the supernatant was collected after filtering through a 40-μm cell strainer. Cells were suspended in PBS containing 3% FBS, and nonspecific binding of the antibodies to Fc receptors was blocked using an Fc receptor-blocking agent (1:50) (BioLegend). Cells were stained with APC-anti-mouse CD11b (1:150), PE anti-mouse F4/80 (1:20), APC-Cy7 anti-mouse Ly6c (1:300) and Alexa488 anti-mouse CD206 (1:50) (BioLegend). The LIVE/DEAD Fixable Aqua Dead Cell Stain Kit (Invitrogen) was used to label dead cells. After washing, cells were analysed using BD FACSVerse. Cell sorting was performed by BD FACSAria II. The data were analysed by Flo Jo software (Tree Star).

Statistical analysis. All values are reported as mean ± s.d. Statistical calculations were performed using GraphPad Prism 6 (GraphPad software Inc.). We analysed the data using the unpaired two-tailed Student's *t*-test (parametric) or the unpaired two-tailed Mann–Whitney *U*-test (non-parametric) in case of analysing two groups. The one-way analysis of variance with Turkey's *post hoc* test (parametric) or the Kruskal–Wallis test with Dunn's correction for multiple comparisons (non-parametric) was used in case of analysing multiple groups. The two-way analysis of variance followed by Sidak's multiple comparisons test was used to compare the effect of multiple levels of two factors. The *F*-test, Browne–Forsythe test or the Bartlett's test was used to determine the distributional assumption (normality and homogeneity of variance) of the data. When the data do not fit a normal distribution, non-parametric tests are used. Significant differences were defined as $P<0.05$.

References

1. Horton, R. GBD 2010: understanding disease, injury, and risk. *Lancet* **380,** 2053–2054 (2012).
2. Kearney, P. M. *et al.* Global burden of hypertension: analysis of worldwide data. *Lancet* **365,** 217–223 (2005).
3. Gibbons, G. H. & Dzau, V. J. The emerging concept of vascular remodeling. *N. Engl. J. Med.* **330,** 1431–1438 (1994).
4. Intengan, H. D. & Schiffrin, E. L. Vascular remodeling in hypertension: roles of apoptosis, inflammation, and fibrosis. *Hypertension* **38,** 581–587 (2001).
5. Li, C. & Xu, Q. Mechanical stress-initiated signal transductions in vascular smooth muscle cells. *Cell Signal.* **12,** 435–445 (2000).
6. Wenzel, P. *et al.* Lysozyme M-positive monocytes mediate angiotensin II-induced arterial hypertension and vascular dysfunction. *Circulation* **124,** 1370–1381 (2011).
7. Hadrava, V. *et al.* Vascular smooth muscle cell proliferation and its therapeutic modulation in hypertension. *Am. Heart J.* **122,** 1198–1203 (1991).
8. Angers, S. & Moon, R. T. Proximal events in Wnt signal transduction. *Nat. Rev. Mol. Cell Biol.* **10,** 468–477 (2009).
9. Clevers, H. Wnt/beta-catenin signaling in development and disease. *Cell* **127,** 469–480 (2006).
10. Logan, C. Y. & Nusse, R. The Wnt signaling pathway in development and disease. *Annu. Rev. Cell Dev. Biol.* **20,** 781–810 (2004).
11. Lustig, B. *et al.* Negative feedback loop of Wnt signaling through upregulation of conductin/axin2 in colorectal and liver tumors. *Mol. Cell. Biol.* **22,** 1184–1193 (2002).
12. Itaranta, P. *et al.* Wnt-4 signaling is involved in the control of smooth muscle cell fate via Bmp-4 in the medullary stroma of the developing kidney. *Dev. Biol.* **293,** 473–483 (2006).
13. Cohen, E. D. *et al.* Wnt signaling regulates smooth muscle precursor development in the mouse lung via a tenascin C/PDGFR pathway. *J. Clin. Invest.* **119,** 2538–2549 (2009).
14. Wang, X. *et al.* A role for the beta-catenin/T-cell factor signaling cascade in vascular remodeling. *Circ. Res.* **90,** 340–347 (2002).
15. Tsaousi, A. *et al.* Wnt4/beta-catenin signaling induces VSMC proliferation and is associated with intimal thickening. *Circ. Res.* **108,** 427–436 (2011).
16. Naito, A. T. *et al.* Complement c1q activates canonical wnt signaling and promotes aging-related phenotypes. *Cell* **149,** 1298–1313 (2012).
17. Petry, F., Botto, M., Holtappels, R., Walport, M. J. & Loos, M. Reconstitution of the complement function in C1q-deficient (C1qa−/−) mice with wild-type bone marrow cells. *J. Immunol.* **167,** 4033–4037 (2001).
18. Letavernier, E. *et al.* Targeting the calpain/calpastatin system as a new strategy to prevent cardiovascular remodeling in angiotensin II-induced hypertension. *Circ. Res.* **102,** 720–728 (2008).
19. Ross, R. The pathogenesis of atherosclerosis: a perspective for the 1990s. *Nature* **362,** 801–809 (1993).
20. Lawrence, M. C. *et al.* The roles of MAPKs in disease. *Cell Res.* **18,** 436–442 (2008).
21. van Noort, M., Meeldijk, J., van der Zee, R., Destree, O. & Clevers, H. Wnt signaling controls the phosphorylation status of beta-catenin. *J. Biol. Chem.* **277,** 17901–17905 (2002).
22. Lepourcelet, M. *et al.* Small-molecule antagonists of the oncogenic Tcf/beta-catenin protein complex. *Cancer Cell* **5,** 91–102 (2004).
23. Wirth, A. *et al.* G12-G13-LARG-mediated signaling in vascular smooth muscle is required for salt-induced hypertension. *Nat. Med.* **14,** 64–68 (2008).
24. van Rooijen, N. & van Nieuwmegen, R. Elimination of phagocytic cells in the spleen after intravenous injection of liposome-encapsulated dichloromethylene diphosphonate. An enzyme-histochemical study. *Cell Tissue Res.* **238,** 355–358 (1984).
25. Mosser, D. M. & Edwards, J. P. Exploring the full spectrum of macrophage activation. *Nat. Rev. Immunol.* **8,** 958–969 (2008).
26. Fujiu, K., Wang, J. & Nagai, R. Cardioprotective function of cardiac macrophages. *Cardiovasc. Res.* **102,** 232–239 (2014).
27. Willert, K. & Nusse, R. Wnt proteins. *Cold Spring Harb. Perspect. Biol.* **4,** a007864 (2012).
28. Yeo, E. J. *et al.* Myeloid WNT7b mediates the angiogenic switch and metastasis in breast cancer. *Cancer Res.* **74,** 2962–2973 (2014).
29. Yoshioka, S. *et al.* WNT7A regulates tumor growth and progression in ovarian cancer through the WNT/beta-catenin pathway. *Mol. Cancer Res.* **10,** 469–482 (2012).
30. Biswas, S. K. *et al.* A distinct and unique transcriptional program expressed by tumor-associated macrophages (defective NF-kappaB and enhanced IRF-3/STAT1 activation). *Blood* **107,** 2112–2122 (2006).
31. Schwartz, S. M., Campbell, G. R. & Campbell, J. H. Replication of smooth muscle cells in vascular disease. *Circ. Res.* **58,** 427–444 (1986).
32. Dzau, V. J., Braun-Dullaeus, R. C. & Sedding, D. G. Vascular proliferation and atherosclerosis: new perspectives and therapeutic strategies. *Nat. Med.* **8,** 1249–1256 (2002).
33. Scott-Burden, T., Resink, T. J., Baur, U., Burgin, M. & Buhler, F. R. Epidermal growth factor responsiveness in smooth muscle cells from hypertensive and normotensive rats. *Hypertension* **13,** 295–304 (1989).
34. Dejana, E. The role of wnt signaling in physiological and pathological angiogenesis. *Circ. Res.* **107,** 943–952 (2010).
35. Bonta, P. I. *et al.* Nuclear receptor Nur77 inhibits vascular outward remodelling and reduces macrophage accumulation and matrix metalloproteinase levels. *Cardiovasc. Res.* **87,** 561–568 (2010).
36. Tieu, B. C. *et al.* An adventitial IL-6/MCP1 amplification loop accelerates macrophage-mediated vascular inflammation leading to aortic dissection in mice. *J. Clin. Invest.* **119,** 3637–3651 (2009).

37. Shagdarsuren, E. *et al.* C1-esterase inhibitor protects against neointima formation after arterial injury in atherosclerosis-prone mice. *Circulation* **117,** 70–78 (2008).
38. Bhatia, V. K. *et al.* Complement C1q reduces early atherosclerosis in low-density lipoprotein receptor-deficient mice. *Am. J. Pathol.* **170,** 416–426 (2007).
39. Botto, M. *et al.* Homozygous C1q deficiency causes glomerulonephritis associated with multiple apoptotic bodies. *Nat. Genet.* **19,** 56–59 (1998).
40. Wessels, M. R. *et al.* Studies of group B streptococcal infection in mice deficient in complement component C3 or C4 demonstrate an essential role for complement in both innate and acquired immunity. *Proc. Natl Acad. Sci. USA* **92,** 11490–11494 (1995).
41. Brault, V. *et al.* Inactivation of the beta-catenin gene by Wnt1-Cre-mediated deletion results in dramatic brain malformation and failure of craniofacial development. *Development* **128,** 1253–1264 (2001).

Acknowledgements

We gratefully acknowledge the gift of the CreERT2 cassette from Dr Pierre Chambon (IGBMC/GIE-CERBM). We would like to thank the following individuals for their technical support: A. Furuyama, M. Ikeda, Y. Ohtsuki, I. Sakamoto, M. Shimizu, H. Taniwaki, R. Takizawa, C. Ogawa, N. Igarashi, Y. Xiao, H. Tomita, M. Hayashi and N. Yamanaka. This work was supported by grants from the Ministry of Education, Culture, Sports, Science and Technology (MEXT); JSPS KAKENHI Grant Number 21229010, and CREST, Japan Science and Technology Agency (to I.K.); JSPS KAKENHI Grant Number 23689038, Sakakibara Memorial Research Grant from the Japan Research Promotion Society for Cardiovascular Diseases, Research Grants from the Japan Prize Foundation, the Uehara Memorial Foundation, the Nakatomi Foundation, Japan Heart Foundation/Novartis, Kanae Foundation for the Promotion of Medical Science, the Japan Foundation for Applied Enzymology and Banyu Research Foundation International (to A.T.N.); JSPS KAKENHI Grant Number 26870141, Japan Heart Foundation/Novartis and Research Grants from the Japan Foundation for Applied Enzymology (to T.S.).

Author contributions

I.K. planned and supervised the project. T.Su., A.T.N., I.S. and I.K. designed the experiments. T.Su., S.N., T.H., A.N., M.I. and T.Y. performed the experiments. K.O., T.Sa., A.H., M.I. and T.Y. analysed data. S.O., T.No. and M.B. contributed new reagents/analytical tools. H.A., T.O., J.-K.L., T.M., Y.K., H.M., I.M. and T.Na. advised on the experiments. T.Su., A.T.N., I.S. and I.K. wrote the manuscript.

Additional information

Supplementary Information accompanies this paper at http://www.nature.com/naturecommunications

Competing financial interests: The authors declare no competing financial interests.

Reprints and permission information is available online at http://npg.nature.com/reprintsandpermissions/

How to cite this article: Sumida, T. *et al.* Complement C1q-induced activation of β-catenin signalling causes hypertensive arterial remodelling. *Nat. Commun.* 6:6241 doi: 10.1038/ncomms7241 (2015).

Heart Vessels
DOI 10.1007/s00380-014-0488-5

ORIGINAL ARTICLE

Coronary atherosclerotic lesions in patients with a ruptured abdominal aortic aneurysm

Atsuko Nakayama · Hiroyuki Morita · Akihiko Hamamatsu · Tetsuro Miyata · Katsuyuki Hoshina · Masatoshi Nagayama · Shuichiro Takanashi · Tetsuya Sumiyoshi · Issei Komuro

Received: 5 November 2013 / Accepted: 14 February 2014

Abstract In this study, the coronary findings in 185 autopsy cases with a ruptured abdominal aortic aneurysm (AAA) from the Tokyo Medical Examiner's Office were examined and compared with those in 1,056 patients undergoing AAA repair at the University of Tokyo Hospital or Sakakibara Heart Institute (Tokyo, Japan). The number of cases with any significant coronary stenosis was significantly greater in the autopsy cases with a ruptured AAA than in the patients undergoing emergency repair of a ruptured AAA, suggesting that the low prevalence of CAD observed in patients undergoing emergency repair of a ruptured AAA was due to the survival bias before reaching hospital. In addition, we also found that significant coronary left main trunk stenosis was more frequent in CAD cases with a ruptured AAA than in those with an unruptured AAA, findings that suggest novel clinical implications. Large-scale prospective studies are warranted to confirm our findings and to clarify the pathophysiological relationship between coronary atherosclerosis and AAA status.

Keywords Abdominal aortic aneurysm · Rupture · Coronary artery · Left main trunk · Mortality

A. Nakayama · I. Komuro
Department of Cardiovascular Medicine, Graduate School of Medicine, The University of Tokyo, Tokyo, Japan

H. Morita (✉)
Department of Translational Research for Healthcare and Clinical Science, Graduate School of Medicine, The University of Tokyo, 7-3-1 Hongo, Bunkyo-ku, Tokyo 113-8655, Japan
e-mail: hmrt-tky@umin.net

A. Hamamatsu
Tokyo Medical Examiner's Office, Tokyo, Japan

T. Miyata · K. Hoshina
Division of Vascular Surgery, Graduate School of Medicine, The University of Tokyo, Tokyo, Japan

M. Nagayama · S. Takanashi · T. Sumiyoshi
Sakakibara Heart Institute, Tokyo, Japan

Introduction

Rupture of an abdominal aortic aneurysm (AAA) is a catastrophic event. Once rupture of an AAA occurs, the mortality rate is extremely high. Even in patients undergoing emergency open repair for a ruptured AAA, the in-hospital operative mortality remains high despite improvements in perioperative management [1]. In our recent retrospective cohort study of more than 1,000 Japanese patients undergoing AAA repair in 2 high-volume hospitals [2], we found that the frequency of coronary artery disease (CAD) in patients receiving emergency repair for a ruptured AAA is significantly less than that in patients receiving elective repair for an unruptured AAA. Since the study population was limited to patients undergoing AAA repair, we had no choice but to guess whether the existence of CAD could increase the liability to circulatory failure followed by death when rupture of an AAA occurred. In order to examine whether these findings are due to "survival bias" or not, the coronary atherosclerotic lesions in patients with a ruptured AAA who died before reaching hospital were evaluated and compared with those in patients undergoing in-hospital AAA repair.

Methods

We conducted a retrospective cohort study of more than 1,000 consecutive patients who underwent emergency or

Published online: 07 March 2014

elective repair for an infrarenal AAA at the University of Tokyo Hospital or Sakakibara Heart Institute Hospital (Tokyo, Japan) from 2003 through 2011. All study participants were of Japanese ancestry. This study was approved by the Ethics Committees of the University of Tokyo Hospital and Sakakibara Heart Institute Hospital. The details of this study have been described elsewhere [2]. Briefly, the indications for and management of AAA repair were determined according to the Japanese Circulation Society Guidelines [3] by the vascular surgery team at each hospital, without any interventions by researchers. AAAs diagnosed as a direct consequence of specific causes such as trauma, infection, inflammatory diseases, and connective tissue disorders (e.g. Marfan syndrome) were excluded from the study in advance. The AAA size of all study participants was evaluated by computed tomography scanning before performing the AAA repair. In the patients receiving elective repair, in principle, preoperative coronary angiography (CAG) was performed <3 months before AAA repair. In those receiving emergency repair, postoperative CAG was performed if they were clinically suspected of suffering from CAD. A case with stenosis >25 % in the coronary left main trunk (LMT) and/or stenosis >50 % in the other coronary segments identified in perioperative CAGs above and/or previous CAGs was defined as a case with significant coronary stenosis, which was reviewed by more than two cardiologists blinded to the study protocol.

Coronary arteries were examined in the hearts of consecutive cases with a ruptured AAA autopsied in the Tokyo Medical Examiner's Office (Tokyo, Japan) from 1995 through 2011. Coronary atherosclerosis was examined by cross-sectional slicing at 3- to 4-mm intervals. The degree of coronary stenosis was classified from 5 to 0 as follows: 5 for total occlusion, 4 for 75–99 % stenosis, 3 for 50–74 % stenosis, 2 for 25–49 % stenosis, 1 for up to 24 % stenosis, and 0 for no atherosclerosis [4]. In this study, categories 2–5 for LMT and/or categories 3–5 for the other coronary segments were defined as significant coronary stenosis in the autopsy cases. These pathological data were only tagged by age and sex. This study was approved by the ethics committee of the Tokyo Medical Examiner's Office.

Statistical analysis was performed with SPSS version 19.0 for Windows (SPSS, Chicago, IL, USA). Baseline characteristics were compared by ANOVA for continuous valuables and the Chi-square test for categorical valuables. Multiple logistic regression analysis was also performed. All tests were two sided with a significance value of $P < 0.05$.

Results

The study population consisted of 866 patients undergoing elective repair of an unruptured AAA, 190 patients undergoing emergency repair of a ruptured AAA, and 185 autopsy cases with a ruptured AAA. Patients receiving AAA repair ($n = 1{,}056$) were 99.4 % identical to the study population in our previous report [2] (Table 1). The distributions of age and sex were similar among the groups. The CAG data from 809 elective repair patients and 84 emergency repair patients as well as the pathological coronary findings from 185 autopsy cases were available.

Cases with any significant coronary stenosis were significantly less frequent in patients undergoing repair of a ruptured AAA [25 (13 %) of 190], compared with patients undergoing repair of an unruptured AAA [479 (55 %) of 866] or autopsy cases with a ruptured AAA [88 (48 %) of 185] ($P < 0.0001$ for each). In an analysis using the number of cases with coronary findings available as a denominator, the same trend was observed ($P < 0.0001$ and $P = 0.006$, respectively) (Table 2). After adjustment

Table 1 Clinical characteristics of patients undergoing repair for infrarenal AAA

	Patients undergoing AAA repair of an unruptured AAA ($n = 866$)	Patients undergoing AAA repair of a ruptured AAA ($n = 190$)	P value
Age (years)	73.3 ± 7.9	73.0 ± 9.4	0.65
BMI (kg/m^2)	22.2 ± 3.5	22.6 ± 3.7	0.16
Male	715 (83 %)	150 (79 %)	0.19
Hypertension	612 (71 %)	122 (64 %)	0.08
Dyslipidemia	409 (47 %)	43 (23 %)	<0.01
Diabetes	228 (26 %)	38 (20 %)	0.07
Current smoker	250 (29 %)	70 (37 %)	<0.01
Hemodialysis	19 (2 %)	6 (3 %)	0.86
Family history of AAA	63 (7 %)	7 (4 %)	0.02
Family history of CAD	122 (14 %)	12 (6 %)	<0.01
Pharmacotherapy			
β, αβ- Blocker	231 (27 %)	54 (28 %)	0.62
ACE inhibitor	83 (10 %)	7 (4 %)	<0.01
ARB	297 (34 %)	66 (35 %)	0.91
Calcium channel blocker	438 (51 %)	75 (39 %)	<0.01
Statin	240 (28 %)	28 (15 %)	<0.01
Laboratory data			
Creatinine (mg/dL)[a]	1.0 ± 0.5	1.3 ± 0.8	<0.01
HbA1c (NGSP) (%)	5.9 ± 0.6	5.9 ± 0.6	0.98

[a] Serum creatinine levels were calculated after excluding the patients receiving hemodialysis. This study population is almost identical to that in our previous study [2]

Table 2 Comparison of the prevalence of coronary atherosclerotic lesions

	Patients undergoing AAA repair of an unruptured AAA ($n = 866$)	Patients undergoing AAA repair of a ruptured AAA ($n = 190$)	Autopsy cases with a ruptured AAA ($n = 185$)	Overall P
Age (years)	73.3 ± 7.9	73.0 ± 9.4	71.7 ± 9.7	0.065
Male (%)	715 (83%)	150 (79%)	138 (75%)	0.110
Cases with significant coronary stenosis (%)	479/866 (55%)	25/190 (13%)	88/185 (48%)	< 0.0001
	$P < 0.0001$	$P < 0.0001$		
	$P = 0.055$			
Cases with significant coronary stenosis divided by cases with coronary findings available (%)	479/809 (59%)	25/84 (30%)	88/185 (48%)	< 0.0001
	$P < 0.0001$	$P = 0.006$		
	$P = 0.004$			

for age and sex, these associations remained statistically significant ($P = 0.003$ and $P = 0.013$, respectively).

In the subanalysis of cases with any significant coronary stenosis, the cases with significant LMT stenosis were significantly more frequent in patients undergoing repair of a ruptured AAA [6 (24 %) of 25] and autopsy cases with a ruptured AAA [41 (47 %) of 88], compared with patients undergoing repair of an unruptured AAA [35 (7 %) of 479] ($P = 0.003$ and $P < 0.0001$, respectively) (Table 3). After adjustment for age and sex, these associations remained statistically significant ($P < 0.0001$ for each). After adjustment for age, sex, body mass index, hypertension, dyslipidemia, diabetes, current smoking, family history of CAD, hypercreatininemia and pharmacotherapy (β, αβ-blocker, ACE inhibitor or ARB, calcium channel blocker and statin), the cases with significant LMT stenosis remained more frequent in CAD patients undergoing repair of a ruptured AAA than in those undergoing repair of an unruptured AAA ($P = 0.014$).

Discussion

In a retrospective cohort study in Japanese patients undergoing repair of AAA in high-volume hospitals, we previously reported that cases with coronary artery disease (CAD) were significantly less prevalent in patients undergoing emergency repair of a ruptured AAA than in those undergoing elective repair of an unruptured AAA [2]. To examine this in greater detail, in this study, the coronary findings in 185 autopsy cases with a ruptured AAA examined by the Tokyo Medical Examiner's Office were compared with those in 1,056 patients undergoing AAA repair. The number of cases with any significant coronary stenosis was significantly greater in the autopsy cases with a ruptured AAA than in the patients undergoing emergency repair of a ruptured AAA, suggesting that the low prevalence of CAD observed in patients undergoing emergency repair of a ruptured AAA was due to the survival bias before reaching hospital. In other words, the existence of CAD could increase the liability to circulatory failure followed by death when the rupture of an AAA occurred.

More importantly, here, we also found significant LMT stenosis was more frequent in the CAD cases with a ruptured AAA than in those with an unruptured AAA. While the prevalence of LMT stenosis in the CAD patients with an unruptured AAA (7 %) was compatible with that in the usual CAD patients, the prevalence in the CAD cases with a ruptured AAA (24 and 47 %) was exceedingly high. The reason for these findings remains unknown, as little is known about the relevance of atherosclerosis to AAA rupture. Indeed, whereas the initiation of AAA onset should be related to the atherosclerotic process, AAA might grow through pathologic mechanisms that differ

Table 3 Comparison of the prevalence of left main trunk (LMT) lesions

	Patients undergoing AAA repair of an unruptured AAA	Patients undergoing AAA repair of a ruptured AAA	Autopsy cases with a ruptured AAA	Overall *P*
Cases with significant coronary stenosis	479	25	88	
Cases with significant LMT stenosis (%)	35 (7.3)	6 (24.0)	41 (46.6)	<0.0001
	$P = 0.003$	$P = 0.043$		
		$P < 0.0001$		
Cases without significant LMT stenosis (%)	444 (92.7)	19 (76.0)	47 (53.4)	<0.0001

from those responsible for atherosclerosis [5, 6]. Further studies that include the vascular development of the coronary arteries and aorta [7] are warranted to clarify the relevance of coronary atherosclerosis to AAA rupture. In particular, if a significant association between LMT stenosis and AAA rupture is established, the silent co-existence of LMT stenosis with AAA should be taken into consideration in the general population.

To the best of our knowledge, this is the first comprehensive study on coronary findings in AAA cases including autopsy cases, providing us with pathophysiological insight into the relationship between coronary findings and AAA. However, there are several limitations. First is the difference in the method used to evaluate the coronary findings. The accuracy of coronary angiograms in comparison with postmortem evaluation was previously validated [8], nevertheless, considering the difference in the definitions of coronary stenosis between CAG and postmortem pathological evaluation, any comparison of coronary findings among groups should be carefully performed. Second, although the autopsy cases consecutively enrolled in this study are expected to be representative of all cases that died of AAA rupture before reaching hospital in the Tokyo district at least with respect to coronary findings, the generalization of our findings to all cases that died of AAA rupture should be performed with caution. In particular, the practical ratio of cases undergoing a postmortem examination to all cases that died of AAA rupture before reaching hospital cannot be precisely estimated. Finally, although the extent of atherosclerotic stenosis was evaluated, the vulnerability of atherosclerotic lesions, which is known to be associated with the clinical outcomes, was not a subject of our study. In spite of these limitations, the data from our large-scale (more than 1,000) analysis including autopsy cases are believed to be clinically valuable. The most impressive message here is that the co-existence of 2 lethal medical conditions—significant LMT stenosis and ruptured AAA—should be taken into consideration. Prospective cohort studies that include the serial evaluation of coronary atherosclerosis as well as aortic properties [9] will confirm our findings.

In conclusion, a high prevalence of left main trunk stenosis was observed in patients with a ruptured infrarenal AAA. Large-scale prospective studies are warranted to confirm our findings and to clarify the pathophysiological relationship between coronary atherosclerosis and AAA status.

Acknowledgments This research is supported by grants-in-aid from the Ministry of Health, Labour and Welfare, Japan (to HM and TM). The authors have no conflicts of interest to declare.

References

1. Bown MJ, Sutton AJ, Bell PR, Sayers RD (2002) A meta-analysis of 50 years of ruptured abdominal aortic aneurysm repair. Br J Surg 89:714–730
2. Nakayama A, Morita H, Miyata T, Hoshina K, Nagayama M, Takanashi S, Sumiyoshi T, Komuro I, Nagai R (2014) Predictors of mortality after emergency or elective repair of abdominal aortic aneurysm in a Japanese population. Heart Vessel 29:65–70

3. (2006) Guidelines for diagnosis and treatment of aortic aneurysm and aortic dissection (JCS 2006) (in Japanese). Circ J 70(Suppl IV):1569–1646
4. Chida K, Ohkawa S, Watanabe C, Shimada H, Ohtsubo K, Sugiura M (1994) A morphological study of the normally aging heart. Cardiovasc Pathol 3:1–7
5. Nakayama A, Morita H, Miyata T, Ando J, Fujita H, Ohtsu H, Akai T, Hoshina K, Nagayama M, Takanashi S, Sumiyoshi T, Nagai R (2012) Inverse association between the existence of coronary artery disease and progression of abdominal aortic aneurysm. Atherosclerosis 222:278–283
6. Brady AR, Thompson SG, Fowkes FG, Greenhalgh RM, Powell JT, UK Small Aneurysm Trial Participants (2004) Abdominal aortic aneurysm expansion: risk factors and time intervals for surveillance. Circulation 110:16–21
7. Tomanek RJ (2005) Formation of the coronary vasculature during development. Angiogenesis 8:273–284
8. Trask N, Califf RM, Conley MJ, Kong Y, Peter R, Lee KL, Hackel DB, Wagner GS (1984) Accuracy and interobserver variability of coronary cineangiography: a comparison with postmortem evaluation. J Am Coll Cardiol 3:1145–1154
9. Oishi Y, Miyoshi H, Iuchi A, Nagase N, Ara N, Oki T (2013) Vascular aging of common carotid artery and abdominal aorta in clinically normal individuals and preclinical patients with cardiovascular risk factors: diagnostic value of two-dimensional speckle-tracking echocardiography. Heart Vessel 28:222–228

Human Molecular Genetics, 2014, Vol. 23, No. 16 **4315–4327**
doi:10.1093/hmg/ddu148
Advance Access published on April 4, 2014

Activating mutations in *RRAS* underlie a phenotype within the RASopathy spectrum and contribute to leukaemogenesis

Elisabetta Flex[1,†], Mamta Jaiswal[3,†], Francesca Pantaleoni[1,‡], Simone Martinelli[1,‡], Marion Strullu[4,7,‡], Eyad K. Fansa[3,‡], Aurélie Caye[4,7], Alessandro De Luca[8], Francesca Lepri[9], Radovan Dvorsky[3], Luca Pannone[1], Stefano Paolacci[1], Si-Cai Zhang[3], Valentina Fodale[1], Gianfranco Bocchinfuso[10], Cesare Rossi[11], Emma M.M. Burkitt-Wright[12], Andrea Farrotti[10], Emilia Stellacci[1], Serena Cecchetti[2], Rosangela Ferese[8], Lisabianca Bottero[1], Silvana Castro[13], Odile Fenneteau[5], Benoît Brethon[6], Massimo Sanchez[2], Amy E. Roberts[14], Helger G. Yntema[15], Ineke Van Der Burgt[15], Paola Cianci[16], Marie-Louise Bondeson[17], Maria Cristina Digilio[9], Giuseppe Zampino[18], Bronwyn Kerr[12], Yoko Aoki[19], Mignon L. Loh[20], Antonio Palleschi[10], Elia Di Schiavi[13,¶], Alessandra Carè[1], Angelo Selicorni[16], Bruno Dallapiccola[9], Ion C. Cirstea[3,21], Lorenzo Stella[10], Martin Zenker[22], Bruce D. Gelb[23,24,25], Hélène Cavé[4,7,§], Mohammad R. Ahmadian[3,§] and Marco Tartaglia[1,§,*]

[1]Dipartimento di Ematologia, Oncologia e Medicina Molecolare and [2]Dipartimento di Biologia Cellulare e Neuroscienze, Istituto Superiore di Sanità, Rome 00161, Italy, [3]Institut für Biochemie und Molekularbiologie II, Medizinische Fakultät der Heinrich-Heine Universitat, Düsseldorf 40225, Germany, [4]Genetics Department, [5]Biological Hematology Department and [6]Pediatric Hematology Department, Robert Debré Hospital, Paris 75019, France, [7]INSERM UMR_S940, Institut Universitaire D'Hématologie (IUH), Université Paris-Diderot Sorbonne-Paris-Cité, Paris 75010, France, [8]Laboratorio Mendel, Istituto di Ricovero e Cura a Carattere Scientifico-Casa Sollievo Della Sofferenza, Rome 00198, Italy, [9]Ospedale Pediatrico 'Bambino Gesù', Rome 00165, Italy, [10]Dipartimento di Scienze e Tecnologie Chimiche, Università 'Tor Vergata', Rome 00133, Italy, [11]UO Genetica Medica, Policlinico S.Orsola-Malpighi, Bologna 40138, Italy, [12]Genetic Medicine, Academic Health Science Centre, Central Manchester University Hospitals NHS Foundation Trust, Manchester M13 9WL, UK, [13]Istituto di Genetica e Biofisica 'A. Buzzati Traverso', Consiglio Nazionale Delle Ricerche, Naples 80131, Italy, [14]Department of Cardiology and Division of Genetics, and Department of Medicine, Boston Children's Hospital, Boston, MA 02115, USA, [15]Department of Human Genetics, Radboud University Medical Centre, and Nijmegen Centre for Molecular Life Sciences, Radboud University, Nijmegen 6500, The Netherlands, [16]Genetica Clinica Pediatrica, Clinica Pediatrica Università Milano Bicocca, Fondazione MBBM, A.O. S. Gerardo, Monza 20900, Italy, [17]Department of Immunology, Genetics and Pathology, Uppsala University, Uppsala 75237, Sweden, [18]Istituto di Clinica Pediatrica, Università Cattolica del Sacro Cuore, Rome 00168, Italy, [19]Department of Medical Genetics, Tohoku University School of Medicine, Sendai 980-8574, Japan, [20]Department of Pediatrics, Benioff Children's Hospital, University of California School of Medicine, and the Helen Diller Family Comprehensive Cancer Center, San Francisco, CA 94143, USA, [21]Leibniz Institute for Age Research, Jena 07745, Germany, [22]Institute of Human Genetics, University Hospital of

*To whom correspondence should be addressed at: Dipartimento di Ematologia, Oncologia e Medicina Molecolare, Istituto Superiore di Sanità, Viale Regina Elena, 299, 00161 Rome, Italy. Tel: +39 0649902569; Fax: +39 0649902850; Email: marco.tartaglia@iss.it
†These authors contributed equally to this project.
‡These authors contributed equally to this project.
¶Present address: Institute of Bioscience and BioResources, Consiglio Nazionale delle Ricerche, Naples 80131, Italy.
§These authors contributed equally as the senior investigators for this project.

Magdeburg, Otto-von-Guericke-University, Magdeburg 39120, Germany, [23]Department of Pediatrics and [24]Department of Genetics and [25]Department of Genomic Sciences, Mindich Child Health and Development Institute, Icahn School of Medicine at Mount Sinai, New York, NY 10029, USA

Received December 10, 2013; Revised and Accepted March 4, 2014

RASopathies, a family of disorders characterized by cardiac defects, defective growth, facial dysmorphism, variable cognitive deficits and predisposition to certain malignancies, are caused by constitutional dysregulation of RAS signalling predominantly through the RAF/MEK/ERK (MAPK) cascade. We report on two germline mutations (p.Gly39dup and p.Val55Met) in *RRAS*, a gene encoding a small monomeric GTPase controlling cell adhesion, spreading and migration, underlying a rare (2 subjects among 504 individuals analysed) and variable phenotype with features partially overlapping Noonan syndrome, the most common RASopathy. We also identified somatic *RRAS* mutations (p.Gly39dup and p.Gln87Leu) in 2 of 110 cases of non-syndromic juvenile myelomonocytic leukaemia, a childhood myeloproliferative/myelodysplastic disease caused by upregulated RAS signalling, defining an atypical form of this haematological disorder rapidly progressing to acute myeloid leukaemia. Two of the three identified mutations affected known oncogenic hotspots of *RAS* genes and conferred variably enhanced RRAS function and stimulus-dependent MAPK activation. Expression of an RRAS mutant homolog in *Caenorhabditis elegans* enhanced RAS signalling and engendered protruding vulva, a phenotype previously linked to the RASopathy-causing SHOC2^{S2G} mutant. Overall, these findings provide evidence of a functional link between RRAS and MAPK signalling and reveal an unpredicted role of enhanced RRAS function in human disease.

INTRODUCTION

Signalling elicited by activated cell surface receptors and transduced through RAS proteins to the RAF/MEK/ERK and PI3K/AKT cascades is central to cell proliferation, survival, differentiation and metabolism (1,2). Owing to this nodal role, enhanced traffic through RAS proteins and their downstream effectors has been established to have a major impact on oncogenesis (3,4). This signalling network also controls early and late developmental processes (e.g. organogenesis, morphology determination, synaptic plasticity and growth), and germline mutations in a number of genes encoding transducers and modulatory proteins participating in the RAS/MAPK signalling pathway have been causally linked to Noonan syndrome (NS) (5), one of the most common diseases affecting development and growth, and a group of clinically related syndromes, the so-called RASopathies (6–8). In this family of disorders, constitutional dysregulation of RAS signalling can be caused by enhanced activation of HRAS, KRAS and NRAS (RAS proteins hereafter), aberrant function of upstream signal transducers or effectors (PTPN11/SHP2, SOS1, SHOC2, RAF1, BRAF, MAP2K1/MEK1 and MAP2K2/MEK2) or inefficient down modulation by feedback mechanisms (CBL, NF1 and SPRED1). More recently, *RIT1*, encoding a monomeric GTPase structurally linked to RAS proteins, was identified as disease gene implicated in NS (9), extending the concept of 'RASopathy gene' to a transducer that contributes to signal propagation through RAS effector pathways but does not belong to the RAS/MAPK signalling backbone.

Clinical manifestations of RASopathies include postnatal reduced growth, a wide spectrum of cardiac defects, facial dysmorphism, ectodermal and skeletal anomalies and variable cognitive deficits (5,8,10). Consistent with the key role of most RASopathy genes in oncogenesis, these disorders are also characterized by variably increased risk for certain haematologic malignancies and other paediatric cancers (6,7,11,12). Most of these conditions are genetically heterogeneous, and the underlying disease gene has not been identified yet for a still significant fraction of cases. Based on the strict mechanistic link between the molecular events controlling development and contributing to oncogenesis, these 'missing' genes represent excellent candidate oncogenes/tumour suppressors.

Here, we report that constitutional dysregulation of RRAS function is associated with a Mendelian trait within the RASopathy spectrum and that somatically acquired mutations in the same gene occur in an aggressive form of juvenile myelomonocytic leukaemia (JMML), a rare childhood myeloproliferative/myelodysplastic neoplasm representing the archetypal somatic RASopathy (13), rapidly progressing to acute myeloid leukaemia (AML). We also demonstrate that RASopathy-causing *RRAS* mutations are activating and promote signalling perturbation by enhancing stimulus-dependent MEK, ERK and, at a lower extent, AKT phosphorylation.

RESULTS

Identification of candidate disease genes and *RRAS* mutation analysis

While the core of the machinery implicated in RAS signalling has been characterized comprehensively, signal propagation through this network is likely to include a larger number of proteins playing a modulatory or structural role (14), whose aberrant or defective function is expected to perturb development and

contribute to oncogenesis. Based on this assumption, we used a protein interaction/functional association network analysis to select a panel of genes encoding proteins functionally linked to the RAS signalling network as candidates for NS or a related RASopathy (15). Candidate gene selection was based on the use of the previously identified RASopathy genes as 'seed' proteins (i.e. proteins used to build the interaction/functional networks), and considering a panel of databases to construct functional subnetworks (Supplementary material, Table S1 and Fig. S1). Sequence scanning of the best candidates in a RASopathy cohort including 96 unrelated subjects negative for mutations in known disease genes allowed the identification of a functionally relevant *RRAS* change (c.163G>A, p.Val55Met) (Supplementary material, Fig. S2) in an adult subject with clinical features suggestive of NS but lacking sufficient characteristics to allow a definitive diagnosis (Supplementary material, Table S2). Parental DNA was not available for segregation analysis. The mutation was not identified among >400 population-matched unaffected individuals, indicating that it did not represent a common polymorphic nucleotide substitution. This change, rs368625677 (dbSNP 138), had been described in 1/13,006 alleles in the NHLBI Exome Sequencing Project (http://eversusgs.washington.edu/EVS/). Of note, similar frequencies have been reported in the same database for recurrent RASopathy-causing mutations (e.g. c.922A>G in *PTPN11*, and c.1259G>A in *CBL*). Mutation analysis was extended to additional 408 patients with NS or a clinically related phenotype tested negative for mutations in the major NS disease genes (see Materials and Methods), allowing to identify one sporadic case heterozygous for a three-nucleotide duplication (c.116_118dup, p.Gly39dup) (Supplementary material, Fig. S2). Parental DNA sequencing of the relevant exon demonstrated the *de novo* origin of the variant, and STR genotyping confirmed paternity. In this subject, the duplication was documented in DNA obtained from skin fibroblasts, excluding a somatic event restricted to haematopoietic cells. The subject had features reminiscent of NS (Fig. 1A and Supplementary material, Table S2), with onset of AML suspected to represent a blast crisis of JMML (Supplementary material, Table S3 and Fig. S3). In this patient, exome sequencing performed on leukaemic and non-leukaemic DNA failed to disclose any additional relevant germline/somatic change affecting genes known to be mutated in RASopathies and JMML, as well as genes directly linked to the RAS signalling network, further supporting the causal role of the identified *RRAS* lesion. Based on this association, the occurrence of *RRAS* mutations was also explored in a panel of genomic DNAs obtained from bone marrow aspirates/circulating leukocytes of 110 subjects with JMML. Heterozygosity for the previously identified Gly^{39} duplication and the c.260A>T (p.Gln87Leu) change was observed in two patients with JMML rapidly progressing to AML (Supplementary material, Table S3 and Fig. S3). Both lesions were absent in non-leukaemic DNA, indicating their somatic origin (Supplementary material, Fig. S2). These subjects also carried a somatic *NRAS* mutation, suggesting that the two hits might cooperate with this particularly severe form of disease. Sequencing of isolated JMML myeloid colonies in patient 14385 showed that *NRAS* and *RRAS* mutations coexisted in the same progenitors but failed to establish their sequence of appearance during leukaemogenesis, not allowing to discriminate whether the latter was involved in initiation or progression of disease.

Structural analyses

RRAS encodes a 23-kD a membrane-bound monomeric GTPase with 55–60% amino acid identity to RAS proteins (16). This highly conserved structure is flanked by a unique 26-amino acid region at the *N*-terminus (Fig. 1B). Similarly to the other RAS family proteins, RRAS binds to GTP and GDP with high affinity and specificity and functions as a molecular switch by cycling between active, GTP-bound and inactive, GDP-bound states (17). RRAS is activated by guanine nucleotide exchange factors (GEFs) in response to signals elicited by cell surface receptors. In the GTP-bound state, two functionally conserved regions, switch I and switch II (Fig. 1B), undergo a conformational change enabling RRAS to bind to and activate effector proteins. This interaction is terminated by hydrolysis of GTP to GDP, which is promoted by GTPase-activating proteins (GAPs) and results in switching towards the inactive conformation. Disease-associated *RRAS* mutations affected residues highly conserved among orthologs and paralogs (Supplementary material, Fig. S4) residing in the GTP-binding pocket (Fig. 1C) and were predicted to be damaging with high confidence (Supplementary material, Table S4). Among them, Gln^{87}, homolog of Gln^{61} in RAS proteins, is directly involved in catalysis (18,19). The p.Gln87Leu substitution had previously been reported as a rare somatic event in lung carcinoma, and mutations affecting Gln^{61} are among the most recurrent oncogenic lesions in *RAS* genes (COSMIC database, http://cancer.sanger.ac.uk/cancergenome/projects/cosmic/). Likewise, p.Gly39dup altered the G1 motif participating in GTP/GDP binding and GTPase activity (Fig. 1B). Within this motif, Gly^{12} and Gly^{13} (Gly^{38} and Gly^{39} in RRAS) represent major mutation hot-spots in human cancer (COSMIC database) and account for the majority of germline *HRAS* mutations causing Costello syndrome (20). Of note, analogous insertions in RAS proteins have been reported in JMML and other malignancies (21–24). In contrast, no somatic/germline *RAS* mutation affecting Val^{29}, homolog of Val^{55} in RRAS, had previously been reported. Val^{55} side-chain is not directly involved in GTP/GDP binding, GTP hydrolysis or interaction with effectors. However, it has been reported that H-bonds are possible between the backbone of Val^{29} in HRAS and GDP/GTP (25). Furthermore, it has been suggested that Val^{29} can play a role in the transition between the GDP- and GTP-bound states (26), as supported by the evidence that the Val29Gly substitution in HRAS accelerates the GDP/GTP exchange *in vitro* (27).

Molecular dynamics (MD) simulations were performed to predict *in silico* the effects of p.Val55Met on the structure and dynamics of RRAS (Fig. 2). The mutation was introduced in the available crystallographic structure of RRAS in complex with GDP and Mg^{2+}, and the system was simulated in water for 200 ns. For comparison, MD simulations were also performed using the wild-type protein, which maintained a stable structure along the whole simulation, as expected (Fig. 2A, left panel). In contrast, a dramatic local structural transition extending up to the switch I region (residues 58–64), which mediates effector binding, was documented for the $RRAS^{V55M}$ mutant, after ~80 ns (Fig. 2A, right panel). This conformational transition resulted in an increased solvent exposure of Met^{55}, in agreement with the higher hydrophilicity of this residue compared with Val, and was accompanied by the formation of a stable

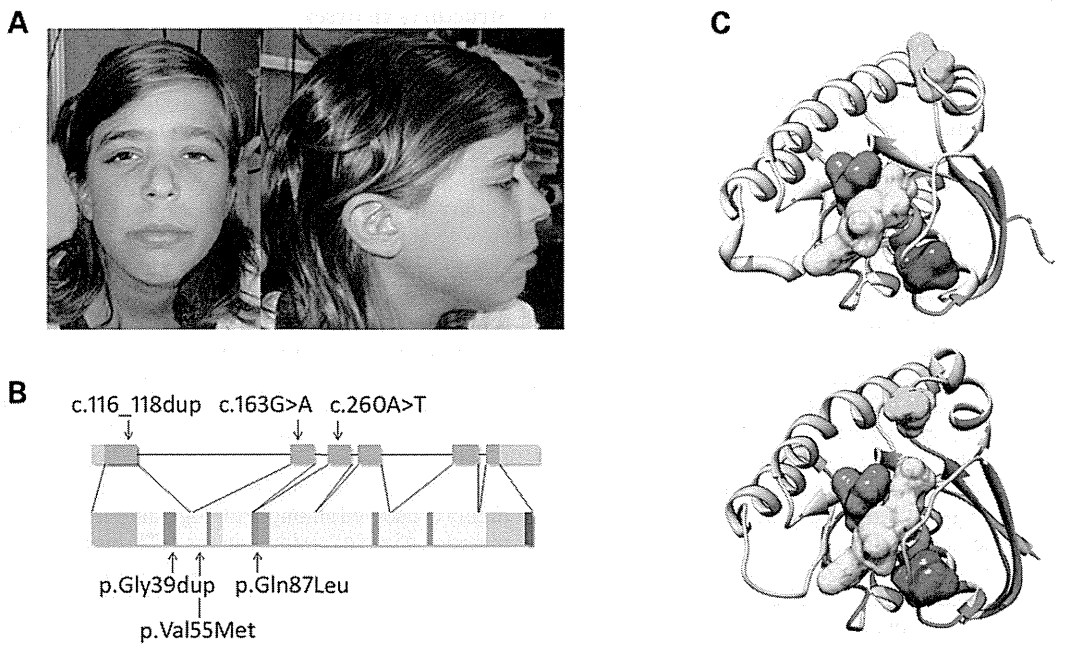

Figure 1. RASopathy-causing and leukaemia-associated *RRAS* mutations. (**A**) Facial features of the affected subject (9802) heterozygous for the *de novo* germline c.116_118dup. (**B**) *RRAS* exon–intron arrangement with coding exons as blue boxes. RRAS functional motifs include the GTP/GDP binding domain (G1 to G5, starting from the *N*-terminus) (red), switch I (light green), switch II (dark green) and hypervariable region (light brown) with the *C*-terminal CAAX motif (dark brown). The unique *N*-terminal region is also shown (violet). Location of disease-associated mutations is reported. (**C**) Position of affected residues on the three-dimensional structure of RRAS in its GDP-bound, inactive state (PDB: 2FN4) (above) and that of non-hydrolysable GTP analogue (GppNHp)-bound, active HRAS (PDB: 5P21) (below). The red surface indicates Gly^{39} and Val^{40} (Gly^{13} and Val^{14}, in HRAS), whereas Val^{55} (Val^{29}) and Gln^{87} (Gln^{61}) are shown in blue and green, respectively. GDP is reported as semi-transparent yellow surface.

cluster involving residues Ile^{50}, Met^{55} and Tyr^{58} (Fig. 2A and Supplementary material, Table S5) permitted by the unbranched and long side-chain of Met^{55}. No further significant conformational changes were observed for the remaining interval of the simulation. The major effect of this structural rearrangement was to increase exposure of GDP to the solvent (Fig. 2B), with an almost doubled solvent accessible surface area of the nucleotide after the conformational transition. This structural rearrangement was accompanied by a perturbation of the intermolecular H-bond network stabilizing GDP binding, with loss of the H-bonds between residues at codons 55 and 56, and GDP (Supplementary material, Table S5). Of note, a possible impact of the described structural transition on RRAS binding to GEF proteins, which bind to this region and mediate GDP release, was also noticed. Specifically, we observed that after the conformational rearrangement, the $RRAS^{V55M}$ region implicated in GEF binding populated a structure similar to that assumed in RAS/GEF complexes (Fig. 2C), suggesting a possible enhanced interaction of the disease-associated RRAS mutant with GEFs. In particular, Tyr^{58} was observed to adopt a side-chain orientation very similar to that of the RAS homolog Tyr^{32} in the HRAS/SOS1 complex, which has been shown to contribute to the structural rearrangements of switch I and interaction with GEFs (28–30).

Overall, these data supported an activating role of p.Val55Met through enhanced GDP release as a result of a decreased affinity for the nucleotide and/or enhanced interaction with a GEF.

Biochemical and functional characterization of RRAS mutants

Previous studies documented the gain-of-function role of p.Gln87Leu on RRAS function, and MAPK and PI3K/AKT signalling (31). To characterize the impact of p.Val55Met and p.Gly39dup on protein function, we analysed the intrinsic and GEF-accelerated nucleotide exchange reaction of these mutants. Dissociation kinetics analysis demonstrated a dramatically increased intrinsic ($RRAS^{G39dup}$) and GEF-stimulated ($RRAS^{G39dup}$ and $RRAS^{V55M}$) dissociation rate of mantGDP, indicating a facilitated nucleotide release in both mutants (Fig. 3A). RAS proteins exhibit low intrinsic GTPase activity that is enhanced by GAPs (32). Assessment of $RRAS^{G39dup}$ and $RRAS^{V55M}$ GTPase activity documented a significantly reduced intrinsic and GAP-stimulated GTP hydrolysis in the former (Fig. 3B and Supplementary material, Fig. S5). Finally, the interaction of RRAS proteins with various effectors was analysed by fluorescence polarization (Fig. 3C). While $RRAS^{WT}$ was found to bind to RAF1, RALGDS, RASSF5 and PLCE1 less efficiently than HRAS, an increased binding affinity to PIK3CA was observed. Compared with $RRAS^{WT}$, aberrant binding behaviour of the two RRAS mutants was demonstrated, with $RRAS^{G39dup}$ exhibiting an increased binding affinity towards PIK3CA, RAF1, PLCE1 and RASSF5, and $RRAS^{V55M}$ to RALGDS.

To gain further insights into the impact of disease-causing mutations on RRAS functional dysregulation and explore their effects on RAS signalling, the activation state of RRAS proteins

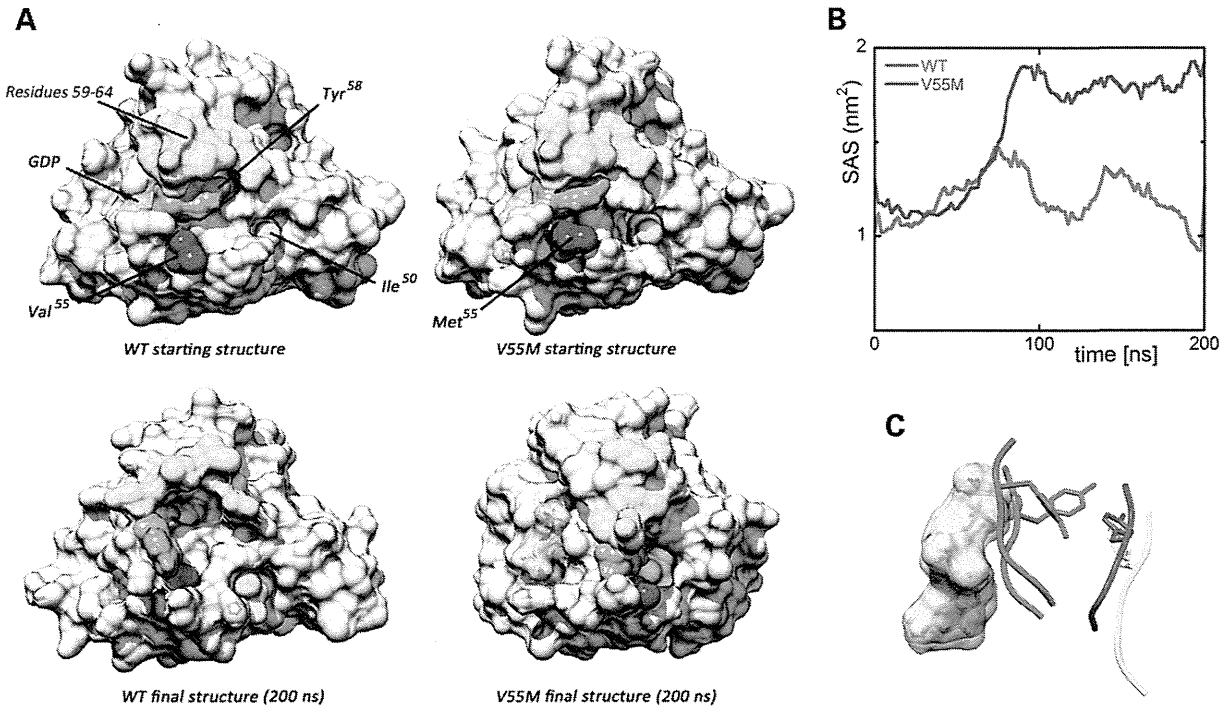

Figure 2. Molecular dynamics (MD) simulations. (**A**) Structural perturbations promoted by the p.Val55Met substitution as obtained from MD simulations of the RRAS/GDP complex. The wild-type (WT) protein is also shown for comparison. Top panels report the protein structures at the beginning of simulations, whereas the final structures (200 ns) are shown at the bottom. The final structure of $RRAS^{V55M}$ is well representative of the last 120 ns of the trajectory. The protein surface of RRAS is shown with GDP (yellow). The mutated residues and those forming a cluster in the simulation of mutated RRAS are coloured as follows: Val^{55}/Met^{55} (blue), Tyr^{58} (pink) and Ile^{50} (cyan). Residues 59–64, which, together with Tyr^{58}, form the switch I region, are coloured in green. (**B**) Solvent accessible surface of GDP in the MD simulations of wild-type (red) and mutant (blue) RRAS/GDP complexes. (**C**) Conformation of the loop comprised between Val^{55}/Met^{55} and Asp^{59} in wild-type (red) and mutant (blue) RRAS/GDP complexes obtained from MD simulations. GDP is reported as semi-transparent yellow surface. Superimposed conformations of the corresponding loop (residues 29–33) in GDP-bound HRAS (violet) (PDB: 4Q21) and GDP-bound HRAS complexed with SOS1 (cyan) (PDB: 1BKD) are shown for comparison. The side chains of Tyr^{58} and the corresponding residue in HRAS, Tyr^{32}, are displayed as sticks.

and extent of signalling through the MAPK and PI3K/AKT cascades were evaluated using transient expression in COS-7 cells. Consistent with the above-mentioned findings, pull-down assays revealed a variably higher proportion of active, GTP-bound form for both mutants (Fig. 4A). Moreover, similarly to what observed under cell-free conditions, $RRAS^{G39dup}$ was resistant to GAP stimulation. Expression of both mutants promoted enhanced serum-dependent MEK, ERK and AKT phosphorylation (Fig. 4B), which was more evident in cells expressing the $RRAS^{G39dup}$ mutant.

Caenorhabditis elegans studies

To explore further the functional impact of the RASopathy causative RRAS mutants on RAS signalling *in vivo*, we used the nematode *C. elegans* as an experimental model. In *C. elegans*, the role of *ras-1*, the *RRAS* ortholog (33), has not been characterized yet. On the contrary, proper signalling through LET-60, the *C. elegans* ortholog of RAS proteins, has been established to play a crucial role in vulval development (34). In particular, LET-60/RAS is known to mediate the priming signal (LIN-3/EGF) released by the anchor cell to induce the three nearby vulval precursor cells (VPCs), P5.p, P6.p and P7.p, to generate a normal vulva. Enhanced and decreased signalling through LET-60 and the MAPK cassette results in multiple ectopic pseudovulvae (multivulva phenotype) and a failure in VPC induction (vulvaless phenotype), respectively (34,35).

Multiple transgenic lines were generated to conditionally express the wild-type *ras-1* cDNA ($ras\text{-}1^{WT}$) or the allele homologous to the disease-associated three-nucleotide duplication ($ras\text{-}1^{G27dup}$), which was identified to occur both as a germline and somatic event. Exogenous RAS-1 expression was induced by heat shock at early L3 larval stage to investigate the effects of the mutant protein on vulval development. Animals expressing $ras\text{-}1^{G27dup}$ displayed abnormal vulval morphogenesis resulting in the formation of a protruding vulva (Pvl) (Fig. 5A and B and Supplementary Material, Table S6), a phenotype associated with aberrant traffic through different signalling cascades (36,37). Of note, this phenotype had previously been reported in worms expressing the RASopathy causative $SHOC2^{S2G}$ mutant (38). Like those animals, $ras\text{-}1^{G27dup}$ worms showed decreased egg-laying efficiency (Egl phenotype), and accumulation of larvae inside the mother (Bag-of-worms phenotype). A significantly less penetrant phenotype was observed in animals expressing $ras\text{-}1^{WT}$. These findings, together with the observation that animals lacking *ras-1* do not exhibit any vulval defect (WormBase, http://www.wormbase.org/, and our personal assessment), supported the gain-of-function role of the mutation on RAS-1 function. At the late L3/early L4 larval stage, vulva

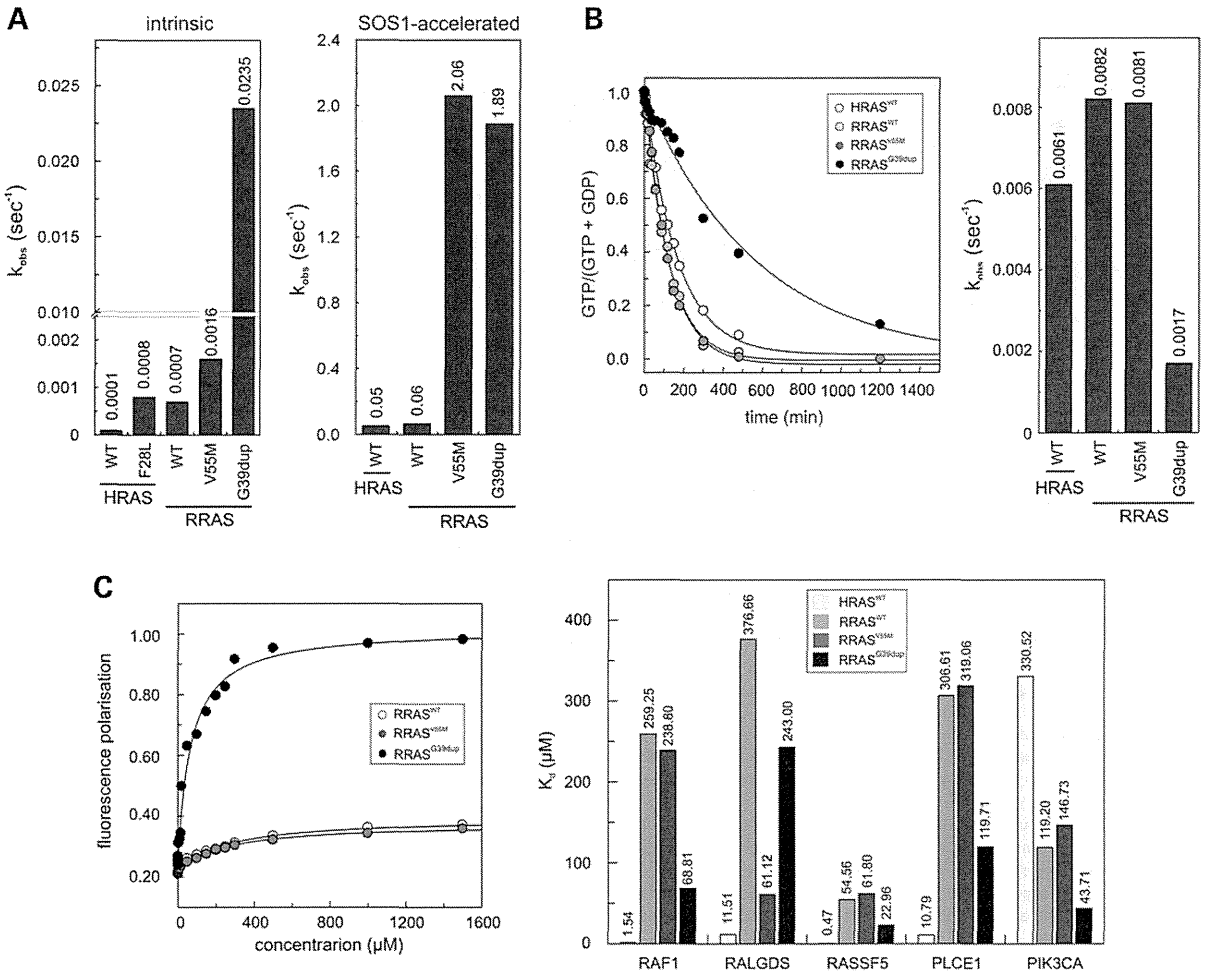

Figure 3. *In vitro* biochemical characterization of the $RRAS^{G39dup}$ and $RRAS^{V55M}$ mutants. (**A**) Intrinsic (left) and SOS1-accelerated (right) mantGDP nucleotide dissociation measured in the presence of 20-fold excess of non-labelled GDP. The decrease in mant fluorescence was fitted by single exponentials to obtain k_{obs} values for nucleotide dissociation. $RRAS^{G39dup}$ exhibited a 35-fold increased intrinsic dissociation of mantGDP, whereas SOS1-accelerated mantGDP dissociation was augmented by ~30-fold for both mutants, compared with $RRAS^{WT}$ and $HRAS^{WT}$. The K_{obs} values are an average of five to seven independent measurements. (**B**) Intrinsic GTP hydrolysis kinetics (left) and rate constants (right) of $RRAS^{G39dup}$ and $RRAS^{V55M}$ proteins, documenting the impaired catalytic activity in the former. The K_{obs} values are an average of five to seven independent measurements. (**C**) Binding of $RRAS^{WT}$, $RRAS^{V55M}$ and $RRAS^{G39dup}$ to the RAS-binding domain of RAF1 measured as variation in fluorescence polarization of each mantGppNHp-bound RRAS protein at increasing concentrations of RAF1-RBD (left), and dissociation constants (K_d) for the interaction of $HRAS^{WT}$ and RRAS proteins to the RBDs of RAF1, RALGDS, PLCE1, PIK3CA and RASSF5 (right). K_d values were obtained by quadratic fitting of the concentration-dependent binding curves from fluorescence polarization measurement as exemplified for RAF1-RBD. Of note, $RRAS^{WT}$ binds to RAF1, RALGDS, RASSF5 and PLCE1 less efficiently than HRAS, whereas an increased binding affinity to PIK3CA is observed.

morphogenesis normally begins with the descendants of VPC P6.p detaching from the cuticle and forming a symmetric invagination (Fig. 5C) (34). Animals in which the expression of *ras-1*^{WT} had been induced at early L3 largely maintained this pattern (17/20). In contrast, in larvae expressing *ras-1*^{G27dup}, descendants of VPCs P5.p and/or P7.p more frequently detached from the cuticle, resulting in larger and more asymmetric invaginations (10/30). This morphogenesis defect was the earliest detectable effect of the *ras-1*^{G27dup} allele on vulval development, similarly to that previously documented in transgenic lines expressing $SHOC2^{S2G}$ (38).

Genetic interaction between the RAS-1/RRAS mutant and LET-60/RAS was also investigated. While expression of the $RAS\text{-}1^{G27dup}$ mutant was able to exacerbate the multivulva phenotype associated with a hyperactive *let-60* allele (*n1046*), expression of wild-type RAS-1 failed to do so (Table 1). Similarly, a significant, although partial rescue of the VPC induction defect associated with a *let-23/EGFR* hypomorphic allele (*sy1*) was observed in animals expressing the activating $RAS\text{-}1^{G27dup}$ mutant, but not in worms expressing the wild-type counterpart (Table 1). Overall, these experiments provided evidence of a positive modulatory role of the RAS-1/RRAS mutant on LET-60/RAS signalling.

DISCUSSION

Mutations of genes coding for proteins with role in RAS signalling and the RAF/MEK/ERK cascade have been identified as the

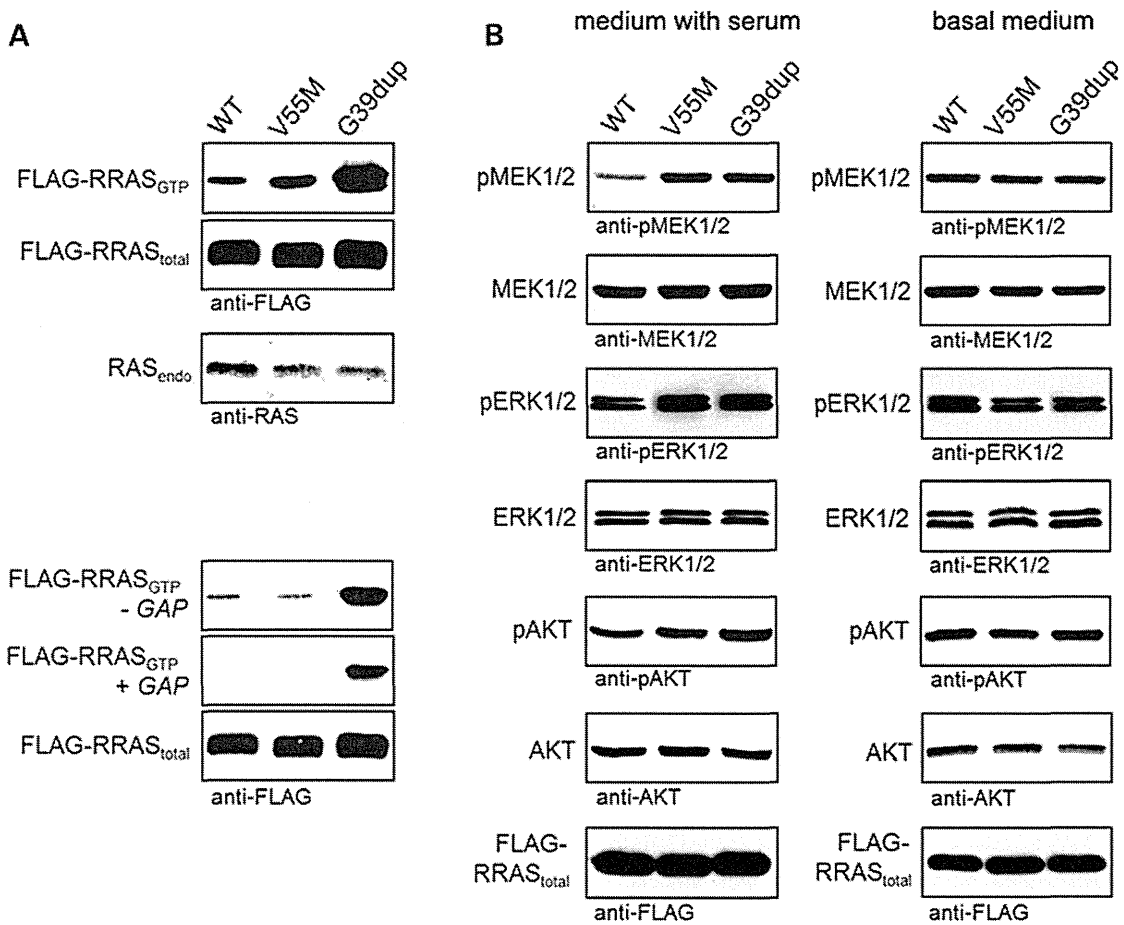

Figure 4. RRAS^{G39dup} and RRAS^{V55M} signalling activities in cells. (**A**) Determination of GTP-bound RRAS levels in COS-7 cells transiently expressing wild-type or mutant FLAG-tagged RRAS proteins. Assays were performed in the presence of serum (above), and in serum-free conditions (−GAP) or in the presence of the neurofibromin GAP domain (+GAP) (below). RRAS^{G39dup} was predominantly present in the active GTP-bound form and was resistant to GAP stimulation, whereas a slightly increased level of GTP-bound RRAS^{V55M} was observed in the presence of serum. Representative blots of three performed experiments are shown. (**B**) Determination of MEK, ERK and AKT phosphorylation levels (pMEK, pERK and pAKT) in transiently transfected COS-7 cells cultured in medium with serum (left) or basal medium (right). Expression of each RRAS mutant resulted in variably enhanced MEK, ERK and also partially AKT phosphorylation after stimulation. Total MEK, ERK and AKT in cell lysates are shown for equal protein expression and loading. Expression levels of exogenous, FLAG-tagged RRAS in cell lysates are shown for each experiment. Representative blots of three performed experiments are shown.

molecular cause underlying a group of clinically related developmental disorders, the RASopathies. Here, we used a gene candidacy approach based on large-scale protein–protein interaction/functional network analysis to identify *RRAS* as a novel gene implicated in a condition with features within the RASopathy spectrum. Disease-causing *RRAS* mutations are activating and act by maintaining the GTPase in its GTP-bound active state. Aberrant RRAS function was demonstrated to perturb variably intracellular signal flow through the RAF/MEK/ERK cascade, and to a certain extent also the PI3K/AKT pathway. Of note, these gain-of-function mutations are likely to define a novel leukaemia-prone condition. Consistent with this view, the same class of *RRAS* lesions was identified to occur as acquired somatic event in JMML, characterizing a subset of this myeloproliferative/myelodysplastic disorder with rapid progression to AML.

RRAS shares several biochemical properties with HRAS, NRAS and KRAS, as well as some common function, including stimulation of cell proliferation, survival and transformation (19,39). Despite these similarities, however, previous observations have emphasized the role of RRAS in cell adhesion, spreading and migration, and its modulatory function on effectors distinct from those used by 'classical' RAS proteins (40,41). While PI3K/AKT has been recognized as a major effector pathway of RRAS, only a minor impact on MAPK signalling had been reported (41,42). The present *in vitro* findings provide evidence that disease-associated RRAS mutants enhance the activation of the MAPK cascade, at least in response to specific stimuli. On the other hand, the identification of *RRAS* as a novel disease gene implicated in a RASopathy disorder further emphasizes the relevance of dysregulated signalling controlling cell spreading and migration in certain features of NS (e.g. congenital heart defects and lymphedema) and JMML (leukocyte infiltration in non-haematopoietic tissues) (43–45).

Caenorhabditis elegans studies provided evidence for a genetic interaction between the RAS-1^{G27dup}/RRAS^{G39dup} and

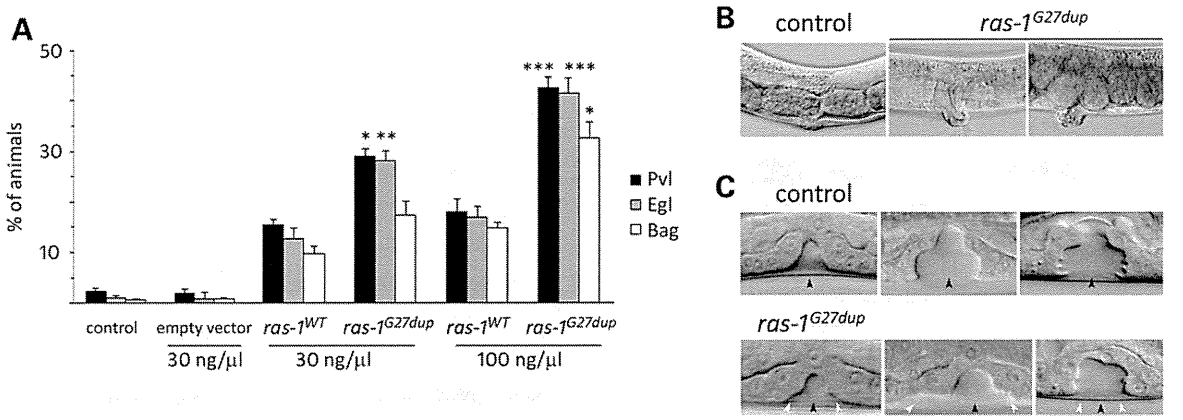

Figure 5. Consequences of *ras-1*^{G27dup} expression on *C. elegans* vulval development. (**A**) Heat-shock-driven expression of *ras-1*^{WT} and *ras-1*^{G27dup} at early L3 stage results in protruding vulva (Pvl), egg laying defective (Egl) and bag-of-worms (Bag) phenotypes. Isogenic animals that had lost the transgene (control group) and worms expressing the heat shock-inducible vector (empty vector) were subjected to heat shock and scored in parallel for comparison. The dose at which the transgene has been injected is reported at the bottom. Error bars indicate SD of three independent experiments. Asterisks indicate significant differences compared with *ras-1*^{WT} at the corresponding dose of injection (*$P < 0.05$; **$P < 0.005$; ***$P < 0.0005$; Fisher's Exact Test). (**B**) A proper vulva develops in heat-shocked control animals (left), whereas a protruding vulva is observed in heat-shocked *ras-1*^{G27dup} young adults (middle) and adult worms (right). (**C**) Nomarski images of vulval precursor cells in late L3 (left), early L4 (middle) and mid-late L4 (right) stages from synchronized animals heat-shocked at early L3. In control animals ($N = 48$), only P6.p descendants invaginate (upper panel), whereas in 10 of 30 analysed *ras-1*^{G27dup}-expressing worms, P5.p and/or P7.p descendants also detach from the cuticle, generating asymmetric invaginations (lower panel). Black arrowheads point to P6.p descendant invagination, whereas white arrowheads point to P5.p and P7.p descendant invagination. Anterior is to the left and dorsal is up, in all images.

LET-60/RAS *in vivo*. Specifically, expression of the RAS-1 mutant protein was able to rescue, in part, the VPC induction defect resulting from a hypomorphic LET-23 mutant and enhanced the multivulva phenotype associated with a LET-60 gain-of-function genetic background. No impact of wild-type RAS-1/RRAS expression was observed in both models. We also observed that worms expressing *ras-1*^{G27dup} displayed abnormal vulval morphogenesis (protruding vulva), possibly resulting from aberrant morphogenetic movements of the VPC descendant cells. Of note, we observed an equivalent phenotype in transgenic lines expressing SHOC2^{S2G} (38) and a PTPN11/SHP2 gain-of-function mutant (our unpublished data), suggesting functional equivalence of these mutants. Genetic studies support the view that these vulva defects arise, in part, through perturbation of signalling mediated by the RHO-related GTPase, RAC, which plays a critical role in vulval morphogenesis (37). This finding is in line with the established role of RRAS on RAC signalling (40,41) and with preliminary data indicating enhanced migration and chemotactic capabilities in cells stably expressing the disease-associated RRAS mutants (our unpublished data).

The biochemical characterization of disease-associated *RRAS* mutations provided strong evidence for the existence of distinct structural and mechanistic effects resulting in an overall enhancement of RRAS signalling. Function of RAS family proteins in signal transduction is controlled by two events, the GDP/GTP exchange and GTP hydrolysis. Any perturbation of these processes can affect dramatically the fine-tuned balance of the GTPase interaction with effectors and signal output. The majority of gain-of-function mutations affecting RAS proteins, including those contributing to oncogenesis, trigger the accumulation of these GTPases in the active state by impairing intrinsic GTPase activity, and/or conferring resistance to GAPs (17). This is also the case of two of the three mutations identified in this study, p.Gly39dup and p.Gln87Leu, the latter corresponding to the p.Gln61Leu in RAS proteins (present study and ref. 18,19). The characterization of the biochemical behaviour of RRAS^{G39dup}, however, also demonstrated a dramatic increase in both the intrinsic and GEF-catalysed nucleotide exchange as a process contributing to the accumulation of this mutant in its GTP-bound state. Aberrant GEF-accelerated nucleotide exchange dynamics was identified as the event driving functional dysregulation in the RRAS^{V55M} mutant, which was documented to be hyper responsive to GEF stimulation, but retained stimulus-dependency. Remarkably, the RRAS^{G39dup} and RRAS^{V55M} mutants were demonstrated to exhibit a diverse binding behaviour to effectors suggesting a differential impact of mutations on downstream signalling cascades, including PI3K/AKT and RALGDS/RAL, whose biological significance and impact, however, require further studies.

The clinical phenotype of the two subjects with germline *RRAS* mutations was reminiscent of NS. The individual with the Gly^{39} duplication displayed pulmonic stenosis, reduced growth, café-au-lait spots, mild motor delay and low-set ears, which recur in NS (5). Facial features, however, were distinctive, and not typical of NS. In contrast, the patient heterozygous for the p.Val55Met substitution exhibited a very mitigated phenotype characterized by suggestive facial characteristics (triangular face, downslanting palpebral fissures and low-set ears), low posterior hairline, broad chest and borderline cognitive abilities, without cardiac involvement or defective growth, indicating that clinical features associated with *RRAS* mutations might be quite subtle. Of note, the milder phenotype associated with the p.Val55Met change is consistent with the weaker perturbing effect of the RRAS^{V55M} mutant on MAPK and PI3K/AKT signalling compared with the RRAS^{G39dup} protein. Additional information on the spectrum of germline *RRAS* mutations, their associated phenotype and their functional impact on signalling,